



## CHARM HADRON PROPERTIES IN 400 GeV/c pp INTERACTIONS

## LEBC-EHS Collaboration

M. Aguilar-Benitez<sup>10</sup>, W.W.M. Allison<sup>12</sup>, J.L. Bailly<sup>11</sup>, S. Banerjee<sup>3</sup>,  
W. Bartl<sup>23</sup>, M. Begalli<sup>1</sup>, P. Beillière<sup>6</sup>, R. Bizarri<sup>15</sup>, H. Briand<sup>14</sup>,  
V. Canale<sup>15</sup>, C. Caso<sup>8</sup>, E. Castelli<sup>22</sup>, P. Checchia<sup>13</sup>, P.V. Chliapnikov<sup>18</sup>,  
N. Colino<sup>10</sup>, R. Contri<sup>8</sup>, D. Crenell<sup>16</sup>, A. De Angelis<sup>13</sup>, L. de Billy<sup>14</sup>,  
C. Defoix<sup>6</sup>, R. DiMarco<sup>17</sup>, E. DiCapua<sup>15</sup>, F. Diez-Hedo<sup>10</sup>, J. Dolbeau<sup>6</sup>,  
J. Dumarchez<sup>14</sup>, M. Ericsson<sup>19</sup>, S. Falciano<sup>15</sup>, C. Fisher<sup>16†</sup>, Yu.V. Fisyak<sup>18</sup>,  
F. Fontanelli<sup>8</sup>, J. Fry<sup>9</sup>, S.N. Ganguli<sup>3</sup>, U. Gasparini<sup>13</sup>, U. Gensch<sup>2</sup>,  
S. Gentile<sup>15</sup>, D.G. Gibaut<sup>12</sup>, A.T. Goshaw<sup>7</sup>, F. Grard<sup>11</sup>, A. Gurtu<sup>3</sup>,  
R. Hamatsu<sup>21</sup>, L. Haupt<sup>19</sup>, S. Hellman<sup>19</sup>, V.P. Henri<sup>11</sup>, J.J. Hernandez<sup>5</sup>,  
T. Hirose<sup>21</sup>, S.O. Holmgren<sup>19</sup>, J. Hrubec<sup>23</sup>, P. Hughes<sup>16</sup>, D. Huss<sup>20</sup>,  
M. Iori<sup>15</sup>, E. Jegham<sup>20</sup>, K.E. Johansson<sup>19</sup>, M.I. Josa<sup>10</sup>, M. Kalelkar<sup>17</sup>,  
I. Kita<sup>21</sup>, A.G. Kholodenko<sup>18</sup>, E.P. Kistenev<sup>18</sup>, S. Kitamura<sup>21</sup>, D. Knauss<sup>2</sup>,  
V.V. Kniazev<sup>18</sup>, W. Kowald<sup>7</sup>, D. Kuhn<sup>23</sup>, P. Ladron de Guevara<sup>10</sup>, M. Laloum<sup>6</sup>,  
P. Legros<sup>11</sup>, H. Leutz<sup>5</sup>, L. Lyons<sup>12</sup>, M. MacDermott<sup>16</sup>, P.K. Malhotra<sup>3</sup>,  
P. Mason<sup>9</sup>, M. Mazzucato<sup>13</sup>, M.E. Michalon-Mentzer<sup>20</sup>, A. Michalon<sup>20</sup>,  
T. Moa<sup>19</sup>, R. Monge<sup>8</sup>, L. Montanet<sup>5</sup>, G. Neuhofer<sup>23</sup>, H.K. Nguyen<sup>14</sup>,  
S. Nilsson<sup>19</sup>, H. Nowak<sup>2</sup>, N. Oshima<sup>21</sup>, G. Otter<sup>1</sup>, R. Ouared<sup>14</sup>,  
J. Panella Comellas<sup>12</sup>, G. Patel<sup>9</sup>, C. Patrignani<sup>15</sup>, M. Pernicka<sup>23</sup>,  
P. Pilette<sup>11</sup>, C. Pinori<sup>13</sup>, G. Pirreda<sup>15</sup>, R. Plano<sup>17</sup>, A. Poppleton<sup>5</sup>,  
P. Poropat<sup>22</sup>, R. Raghavan<sup>3</sup>, S. Reucroft<sup>5</sup>, K. Roberts<sup>9</sup>, W.J. Robertson<sup>7</sup>,  
H. Rohringer<sup>23</sup>, J.M. Salicio<sup>10</sup>, R. Schulte<sup>1</sup>, B. Sellden<sup>19</sup>, M. Sessa<sup>22</sup>,  
F. Simonetto<sup>13</sup>, S. Squarcia<sup>8</sup>, P. Stamer<sup>17</sup>, V.A. Stopchenko<sup>18</sup>,  
A. Subramanian<sup>3</sup>, W. Struczinski<sup>1</sup>, K. Takahashi<sup>21</sup>, S. Tavernier<sup>4</sup>,  
M.C. Touboul<sup>14</sup>, U. Trevisan<sup>8</sup>, C. Troncon<sup>22</sup>, T. Tsurugai<sup>21</sup>, L. Ventura<sup>13</sup>,  
P. Vilain<sup>4</sup>, C. Voltolini<sup>20</sup>, B. Vonck<sup>4</sup>, W.D. Walker<sup>7</sup>, C.F. Wild<sup>7</sup>,  
T. Yamagata<sup>21</sup>, T.P. Yiou<sup>14</sup>, G. Zumerle<sup>13</sup>

We dedicate this work to our colleague Colin Fisher who died tragically on February 11, 1988.

Submitted to Zeitschrift für Physik C

† Deceased.

- 1 III Physikalisches Institut der Technischen Hochschule, D-1500 Aachen,  
Federal Republic of Germany
- 2 Institute für Hochenergiephysik de AdW der DDR, DDR-1615 Berlin-Zeuthen,  
German Democratic Republic
- 3 Tata Institute of Fundamental Research, Bombay 400005, India
- 4 IIHE ULB-VUB, B-1050 Brussels, Belgium
- 5 CERN, European Organization for Nuclear Research, CH-1211 Geneva 23,  
Switzerland
- 6 Lab. de Physique Corpusculaire, Collège de France, F-75231 Paris, France
- 7 Duke University, Durham, NC 27706, USA
- 8 Dipartimento di Fisica and INFN, Università di Genova, I-16146 Genova,  
Italy
- 9 Physics Department, University of Liverpool, Liverpool L693BX, UK
- 10 Division of Particle Physics, CIEMAT-JEN, E-28040 Madrid, Spain
- 11 Université de l'Etat à Mons, B-7000 Mons, Belgium
- 12 Nuclear Physics Laboratory, University of Oxford, Oxford OX13RH, UK
- 13 Dipartimento di Fisica, Università di Padova and INFN, I-35131 Padova,  
Italy
- 14 LPNHE, Paris 6-Paris 7, F-75231 Paris, France
- 15 Dipartimento di Fisica and INFN, Università di Roma, La Sapienza,  
I-00185 Roma, Italy
- 16 Rutherford and Appleton Laboratory, Chilton OX110QX, UK
- 17 Rutgers University, New Brunswick, NJ 08903, USA
- 18 Institute for High Energy Physics, Serpukhov, SU-142284 Protvino, USSR
- 19 Institute of Physics, University of Stockholm, S-11346 Stockholm, Sweden
- 20 Div. High Energy, CRN Strasbourg and Université Louis Pasteur, F-67037  
Strasbourg, France
- 21 Tokyo University of Agriculture and Technology and Tokyo Metropolitan  
University, Tokyo, 158 Japan
- 22 Dipartimento di Fisica and INFN, Università Trieste, I-34100 Trieste  
Italy
- 23 Inst. für Hochenergiephysik der Österreichischen Akademie de  
Wissenschaften, A-1050 Wien

### ABSTRACT

A study of the properties of charm particles produced in 400 GeV/c pp interactions is reported. The experiment was performed using the high resolution hydrogen bubble chamber LEBC in association with the European Hybrid Spectrometer at the CERN SPS. Details of the experimental set-up and operational procedures are given and the methods to extract samples of charm decays are discussed. Results are presented on the intrinsic properties of charm particles (masses, lifetimes, decay modes and branching ratios), adding, whenever appropriate, the relevant information obtained in a similar study made with 360 GeV/c  $\pi^-p$  interactions. The hadroproduction properties of charm states (total and differential cross sections, correlations) are presented and discussed in the context of current QCD inspired phenomenology.

## 1. INTRODUCTION

Charm physics was born, experimentally, with the discovery in 1974 of the  $J/\psi$  particle in hadron-hadron interactions and electron-positron annihilations. Since then, intensive experimental effort has been devoted to understanding the spectroscopy of the charm states and the dynamics behind the production of particles with a charm quark content in weak, electromagnetic and strong interactions.

It has been recognized that the physics of charm particles represents an excellent laboratory for the study of detailed features of the weak interaction governing the decay mechanism of these states, as well as for a deeper understanding of several aspects of quantum chromodynamics. In this context it is worthwhile to recall that the observation of different lifetimes for the charged and neutral ground states of the D mesons has been very relevant in the discussion of the underlying decay diagrams and their relative contributions. On the other hand, the determination of the inclusive total and differential hadroproduction cross sections of charm particles and their energy dependence, is most important when trying to establish the size of the contributions of the various basic QCD subprocesses among the fundamental parton constituents (gluons and quarks).

Despite much experimental activity the detailed knowledge of charm particles, at the level of both the intrinsic properties (masses, lifetimes, decay modes, branching ratios...) and of those depending on the production mechanisms (total and differential cross sections, correlations...) is still unsatisfactory. Among the meson charm states only the SU(4) multiplet of pseudoscalar states has all its members identified, the situation in the baryon sector being more dramatic with the fundamental SU(4) 20-plets still incomplete. There is clearly no need to stress the precarious situation of experimental information relevant to the study of the production properties.

To overcome existing limitations, a large variety of experimental approaches have been developed in the past few years. The use of a small, high resolution, rapid cycling liquid hydrogen bubble chamber, coupled to a large acceptance spectrometer able to measure precisely and to identify photons, electrons and hadrons has proven to be a most valuable technique.

It has lead, through accurate measurements with small and controlled systematic errors, to a significant improvement in the knowledge of basic properties of charm particles. The first indisputable observation of the intriguing difference between the charged and neutral D meson lifetimes was provided by the NA16 experiment performed by the LEBC-EHS collaboration [1]. Moreover, the first non controversial quantitative statement concerning the size of the hadroproduction cross sections at high energies was also made by this experiment [2], which also gave information on branching ratios [3].

In this paper we summarize the main results obtained in the last experiment, called NA27, performed by the LEBC-EHS collaboration at the CERN SPS. The production and decay properties of charm particles produced in proton-proton interactions will be presented, and compared or combined when appropriate, with existing data obtained by this experiment in a previous  $\pi^-$  exposure [4].

A brief description of the experimental set up is given in Section 2. The data reduction process leading to the selection of clean charm samples is summarized in Section 3. The results on the properties of the D meson states are given in Section 4. The status of our understanding of the properties of the  $\Lambda_c$  baryon and  $D_s$  meson appears in Sections 5 and 6 respectively. Section 7 is devoted to a phenomenological, QCD inspired, discussion of the observations made in the sector of D meson production. Some concluding remarks are contained in Section 8.

## 2. EXPERIMENTAL SET-UP

The experimental set-up is shown in Fig. 1 and has been extensively described elsewhere [5]. We will briefly summarize here the main features.

LEBC is a rapid cycling liquid hydrogen bubble chamber, with a fiducial volume of  $12 \times 5 \times 2.5$  cm<sup>3</sup>, which was photographed by two cameras with a demagnification of 0.89 on 50 mm film. Tracks in LEBC have a bubble density of  $80$  cm<sup>-1</sup>, with a bubble diameter of 17  $\mu$ m. The direct observation of the production and decay vertices in LEBC is one of the key features of this experiment. It allows the off-line selection of the charm candidates with

high efficiency (see section 3.2), and reduces the background by several orders of magnitude. Fig. 2 shows a LEBC picture and a computer treated image of the digitizings of a pp interaction with production of two charm particles.

The spectrometer consists of three parts. Immediately downstream of the bubble chamber there is the so called zeroth lever arm with two wire chambers W0 and W1 and two small drift chambers MDC1 and MDC2. W0 and W1 are used for track reconstruction and for triggering purposes. An interaction trigger is defined by requiring more than two hits in each of these two wire chambers. This trigger accepted  $(80.3 \pm 4.5)\%$  of the inelastic cross section and  $(98 \pm \frac{2}{3})\%$  of the charm events.

Each of the two additional lever arms includes a magnet and three large drift chambers (M1, M2 and D1-D6 in Fig. 1). The drift chambers have four wire planes. The space point reconstruction precision is better than 500  $\mu\text{m}$ . The single plane is 90% efficient.

M1 is a superconducting magnet located 2.7 m downstream of LEBC. The field at the center is set to 0.8 T and the momentum kick in the bending plane is 480 MeV/c. M2 is a conventional magnet located 18 m further downstream and giving a momentum kick of 450 MeV/c. Both magnets have the main field axis in the z-direction (perpendicular to the beam and in the horizontal plane). Two proportional inclined chambers (PIC12 and PIC34) are installed in the center of the magnet M1.

Slow particles, which are strongly deflected by the magnet M1, are usually measured from the hits recorded in the multiwire proportional chamber W2, close to the magnet. Particles with momenta in the range 1 - 30 GeV/c traverse all (or part of) the first lever arm and their trajectories are measured by the drift chambers D1 - D3. In the momentum range above 10 GeV/c, the magnet M2 and the drift chambers D4 - D6 in the second lever arm provide additional momentum measurement. The momentum resolution thus achieved is better than 1% ( $\Delta p/p$ ) over the full range.

The spectrometer contains two electromagnetic calorimeters, the Intermediate Gamma Detector (IGD) and the Forward Gamma Detector (FGD). IGD is behind the last drift chamber D3 of the first lever arm. It is made of

1129 lead glass blocks (15 radiation lengths) with 5x5 cm<sup>2</sup> cross section and has a 35x85 cm<sup>2</sup> hole in the centre to allow forward particles to reach the second lever arm.

FGD is located near the end of EHS and covers the projected image of the IGD hole. It contains a lead glass converter wall (4.7 radiation lengths), a scintillator hodoscope with three planes of 1.5 cm wide fingers to measure the shower position and an absorber wall of 112 lead glass blocks (24 radiation lengths).

The energy resolution is  $\Delta E/E = 0.15/\sqrt{E} + 0.02$  for the IGD and  $\Delta E/E = 0.10/\sqrt{E} + 0.02$  for the FGD, where E is in GeV. The single shower accuracy is about 3 mm for both detectors, resulting in a FWHM of 20 MeV/c<sup>2</sup> for the  $\pi^0$  mass peak in the  $\gamma\gamma$  distribution.

Behind each electromagnetic calorimeter there is an iron-scintillator hadron calorimeter. The Intermediate Neutral Calorimeter (INC), at the end of the first lever arm, is composed of 24 cells, arranged to leave a 40x100 cm<sup>2</sup> hole that matches the acceptance of the second lever arm. The transverse size of the cells is 41x16 cm<sup>2</sup> on the sides and 16x33 cm<sup>2</sup> at the top and bottom. Each cell is made of 12 massive, 5 cm thick iron plates, interleaved with 2 cm plastic scintillators. The iron corresponds to 3.6 interaction lengths and the lead glass in the IGD adds another interaction length, in fact 60% of the hadronic showers are initiated in the IGD. The energy resolution of the INC (combined with IGD) is  $\sigma(E) = 1.52/\sqrt{E}$ , where E is in GeV.

The Forward Neutral Calorimeter (FNC) is designed to absorb 95% of the showers produced by the hadrons reaching it. This is achieved with 80 cm of iron and the lead glass of the FGD, corresponding to 4.8 and 1.5 interaction lengths respectively. The FNC has 10x20 cells covering a total area of 1.5x3.0 m<sup>2</sup>. A cell of 1.14 m length consists of 16 iron plates, 15x15x5 cm<sup>3</sup>, separated by 2 cm thick plexipop scintillator. The energy resolution of the FNC (combined with FGD) is  $\sigma(E) = 1.21/\sqrt{E}$ , where E is in GeV.

Charged particle identification is provided by four different detectors which make use of several techniques to cover the entire momentum range.

The Silica Aerogel Detector (SAD) is a Cerenkov detector located 5 m downstream of LEBC. The detector covers  $1.15 \times 2.94 \text{ m}^2$ , except for a hole in the center to let forward particles go through. The refractive index of the silica aerogel is 1.031, giving threshold momenta of 0.56, 2.0 and 3.8 GeV/c for pions, kaons and protons respectively. The average light yield is 5.5 photoelectrons.

ISIS (Identification of Secondaries by Ionization Sampling) is a drift chamber with a  $40 \text{ m}^3$  fiducial volume which plays a most important role in the reconstruction of tracks and in the identification of charged particles. The drift volume is divided into two drift spaces by a single horizontal wire plane at half the chamber height about 15 cm above the beam axis. A uniform 500 V/cm drift field gives the electrons a drift velocity of 2 cm/ $\mu\text{s}$ . There are 640 anode wires connected in pairs to multihit electronics which give the x and y coordinates and dE/dx measurements of up to 320 points for each track. Straight tracks through the measured points are obtained with a filtering program and the ionization is obtained by comparing the measured pulse heights with a model dE/dx distribution.

e/ $\pi$  separation is obtained in the momentum range 2 - 25 GeV/c,  $\pi$ /K in the range 4 - 30 GeV/c and K/p in the range 7 - 40 GeV/c, where separation means that more than 50% of the particles are uniquely identified when rejecting competing hypotheses with probability below 1%. Choosing the highest probability leads to the right mass assignment for 87% of the tracks.

The Forward Cerenkov (FC) is located in the second lever arm between the drift chambers D4 and D5. It is 12 m long and covers an area of  $2 \times 1 \text{ m}^2$ . The light is collected by 14 concave mirrors ( $28.6 \times 52.0 \text{ cm}^2$  each) with a radius of curvature of 2 m. These mirrors are arranged in a  $2 \times 7$  matrix in the rear plane of the device, where the Cerenkov light is focused on photomultipliers. The radiator is helium at room temperature, refractive index  $\approx 1 + 35 \times 10^{-6}$ , which corresponds to thresholds of 17, 60 and 112 GeV/c for  $\pi$ , K and p respectively.



The Transition Radiation Detector (TRD) is located between the drift chambers D5 and D6. It has 20 units of radiators combined with multi-wire proportional chambers. The radiators consist of carbon fibres of 7  $\mu\text{m}$  diameter and 5 - 7 mm length. The radiator material amounts to 14% of a radiation length or 10% of an interaction length. The probability for correct pion identification increases from 90% at 100 GeV/c to about 98% above 200 GeV/c.

### 3. DATA SELECTION

#### 3.1 DATA CONVENTIONS

We call "charm event" a proton-proton interaction where at least one charm decay is observed. The following conventions are used: decays are labelled  $C_n$ ,  $V_n$  or  $X_n$ , C for a charged decay, V for a neutral decay and X for a topologically ambiguous decay; n is the number of charged tracks for a  $C_n$  and  $V_n$  and it is the minimum number of charged tracks for an  $X_n$ . For each charged decay track, the "impact parameter",  $y$ , at the primary vertex is defined by  $y = L \sin \phi$  (Fig. 3a). For an interaction with one or several associated decays, the largest impact parameter,  $y_M$ , is a good measure of the visibility; normally a cut on this parameter is imposed to ensure high detection efficiency. The smallest impact parameter,  $y_m$ , gives a measure of the clearness of the topology and a cut on this quantity is used to guarantee an unambiguous topology.

#### 3.2 SCANNING AND MEASURING

The event selection starts with the visual scanning of the LEBC pictures. In the first scan, every picture is scanned by operators in two views and with two magnifications (x10 and x30). A prediction for the position of the interacting beam track is obtained from the upstream wire chambers. When an interaction is found, a 4 mm wide scan box (Fig. 3b) centered around the beam is searched for decays and secondary interactions. A second scan is made on frames with an interaction found in the first scan. A third scan is made by physicists on events containing at least one secondary activity in the scan box, or when the first two scans give different results.

The efficiency to find an interaction is very close to 100%, and the double scan efficiency to find secondary activities, including charm decays, is greater than 98%.

In charm events, decay tracks and vertices are often obscured by the forward cone of particles produced at the primary interaction; however, the decays may still be resolved due to the detection of significantly large impact parameters and constraints in the number of tracks. We estimate the finding efficiency to vary between 85 and 95%, depending on the topology. These efficiencies also depend on the cuts applied (different cuts are used for different event types). After a first measurement and processing through the reconstruction programs, events are kept if they contain at least one decay which satisfies the following conditions:

- a) The decay is inside a cylinder with radius  $R$ , centered around the incident beam particle (the charm box).
- b) The decay length is less than  $L$ .
- c) All impact parameters are less than  $T$
- d) The number of decay tracks outside the spectrometer acceptance is less than  $N$ .
- e) At least one track for the V2, X2 topologies and the unique track of the C1, X1 has a  $p_T$  greater than 250 MeV/c ( $p_T$  is the momentum of the secondary particle perpendicular to the time of flight of the parent).

The values of these parameters depend on the topology and are given in Table 1. Cuts a), b) and c) reject most of the non-charm background without affecting the charm sample itself. Cut d) ensures good momentum analysis of the decay. Cut e) is introduced to further reduce the strange particle background which is the dominant one for the V2 and C1 topologies. Decays giving fits to strange particle hypotheses in the subsequent kinematic analysis are removed from the sample. Finally, the remaining charm candidates are remeasured on a single high precision measuring machine, an

HPD, to guarantee uniform high quality processing of all the charm candidates found at the various laboratories in the collaboration.

The HPD [6] is a high precision device, which automatically digitizes the bubble positions. Interactive graphical treatment of the HPD digitizations provides accurate vertex determination, correct association of tracks and vertices and therefore very good assignment of decay topologies. The r.m.s. of the residuals to a straight line fit is  $1.8 \mu\text{m}$  with an average track length in the bubble chamber of 5 cm. After reconstruction of a primary vertex, the error (FWHM) on the impact parameter to that vertex is found to be  $2.5 \mu\text{m}$ ; this enables us to recognize decay tracks with non-zero impact parameters, down to  $7 \mu\text{m}$ , with high efficiency ( $\sim 3\sigma$ ).

From a total of 2,220,000 triggered bubble chamber pictures, 1,015,000 contained a primary proton interaction in the fiducial volume. These interactions correspond to a triggered inelastic cross section of 26.4 mb, giving a total sensitivity of  $(38.5 \pm 1.1)$  events/ $\mu\text{b}$ . By inspection of these interactions on LEBC pictures and applying the geometrical selection criteria a), b), c), approximately 5,000 interactions with a secondary activity were selected. After the first measurements the cuts d) and e) reduced to 720 the number of interactions sent to HPD for precision measurements. The complete analysis, explained below, reduced this sample to 324 events containing 557 observed and accepted charm decays. The previous  $\pi^-p$  experiment in the LEBC-EHS set-up [4] consisted of 850,000 triggered bubble chamber pictures, giving 265,000 primary proton interactions, corresponding to a total sensitivity of  $(15.8 \pm 0.8)$  events/ $\mu\text{b}$ . The final data sample was made of 114 events containing 183 charm decays.

### 3.3 RECONSTRUCTION AND IDENTIFICATION OF THE CHARM DECAYS

The geometrical reconstruction, particle identification and kinematical fitting processes have been described in detail in ref. [5]. It is important to recall that 70% of all tracks and almost 100% of those with  $x_F > 0$  are inside the spectrometer acceptance and that the efficiency for linking bubble chamber tracks to spectrometer tracks is found to be 96% in the region  $x_F > 0$ . The acceptance for D-mesons decaying into all charged particles rises steeply around  $x_F = 0$  to almost 100% and remains at this level

over the whole positive  $x_F$  range. Fig. 4 shows, as an example, the spectrometer acceptance for neutral D mesons giving three constraint fits.

The reconstruction efficiency for  $\pi^0$  with momentum larger than 30 GeV/c is larger than 90%. Below 30 GeV/c the efficiency depends on the production angle of the  $\pi^0$ . Particle identification criteria, namely the acceptance, a figure of merit and a momentum range for the different detectors are given in Table 2. The acceptance is defined as the number of tracks with particle identification information, divided by the number of reconstructed tracks with a hit in W2 (for first lever arm detectors) or D4 (for second lever arm detectors). The figure of merit is the number of tracks with reliable identification information divided by the number of tracks with a signal in the detector. The momentum range gives approximate limits for discrimination between particles.

The decay hypotheses for charm events are selected using the following criteria for the mass assignments of the tracks:

a) ISIS

For tracks with more than 100 ionization measurements, mass hypotheses are accepted if the probability is  $> 4\%$ . For tracks with less than 100 measurements the probability cut is  $1\%$ .

b) SAD

A mass hypothesis is vetoed if the momentum is below threshold and if there is a signal corresponding to  $> 0.5$  photoelectrons.

c) FC

Mass hypotheses are accepted when the probability is  $> 5\%$ . Moreover, when light is seen ( $> 0.1$  photoelectrons) those hypotheses for which no light is expected (i.e. momentum below threshold) are vetoed.

d) TRD

Mass hypotheses are accepted when the probability is  $> 5\%$ .

e) Calorimeters

Hypotheses with probability  $< 0.1\%$  are vetoed.

Kinematical fits are tried for hypotheses compatible with the topology and for all mass assignments of the charged secondary particles not vetoed by particle identification. One and two  $\pi^0$  final state hypotheses are tried whenever the  $\pi^0$ 's have been reconstructed. Missing  $\pi^0$  hypotheses are also attempted, even when  $\pi^0$ 's are not reconstructed. At this level of the analysis, a neutral charm candidate is assumed to be a  $D^0$  or a  $\bar{D}^0$ , whereas for charged decays three hypotheses are tried, i.e.  $D^\pm$ ,  $\Lambda_c^\pm$ ,  $D_s^\pm$ . Cabibbo favoured and unfavoured hypotheses are treated equally. Then a selection among the kinematical fits is performed according to the following criteria:

- a) For 3C (3 constraints) fits we require a fit probability larger than 0.1%.
- b) For 2C/1C fits we require a fit probability larger than 1%.
- c) 3C Cabibbo unfavoured solutions are kept if there are no 3C Cabibbo favoured fits. However, an exception to this rule is made when it leaves only  $D_s$  and  $\Lambda_c$  solutions. In such cases the otherwise rejected Cabibbo unfavoured D decays are kept.
- d) When a kinematic solution requires the presence of unseen neutral particles (0C fit), the quantity:

$$M^2 = m_i^2 + m_f^2 - 2m_i(m_f^2 + p_t^2)^{1/2}$$

is evaluated, where  $m_i$  is the mass of the incident charm particle,  $m_f$  the effective mass of the charged final state and  $p_t$  the transverse momentum of this system. Solutions with one  $\pi^0$  (two  $\pi^0$ 's) are accepted if  $M + \Delta M < 400 \text{ MeV}/c^2$  ( $M - \Delta M > 400 \text{ MeV}/c^2$ ). The same procedure is used to separate  $K^0$  from  $(K^0 + \pi^0)$  solutions using a cut at  $700 \text{ MeV}/c^2$ .

In addition, solutions requiring unseen  $\pi^0$ 's,  $K^0$ 's or neutrons are rejected if these neutral particles are within the acceptance and momentum range where the corresponding calorimeters have a high efficiency to detect them.

For the decays with remaining ambiguities, but where the  $x_F$  of all acceptable solutions differed by less than 0.1, the closest fit to the central value was chosen to represent the decay. Monte Carlo simulations have shown that this has a negligible effect on all physical parameters considered.

This analysis results in a sample of 324 events which contain 557 charm decays. We have estimated that the non-charm background (rare strange particle decays, secondary interactions) is less than 2 decays. 482 charm decays fulfil all the selection criteria discussed above, 425 of them having a clear topology whereas 57 have an ambiguous one. The remaining 75 decays are most probably charm (they have no strange particle fit, their length distribution follows the one expected for charm and they are paired to a charm decay) but they cannot be fully ascertained as such. The 425 charm decays are distributed into 64 C1, 134 C3, 7 C5, 166 V2, 52 V4 and 2 V6.

#### 4. D-MESON PRODUCTION AND DECAY PROPERTIES

##### 4.1 D AND D\* TOTAL CROSS SECTIONS

The cross sections for D/ $\bar{D}$  meson production, where D/ $\bar{D}$  means D or  $\bar{D}$  production, were calculated using a procedure which minimizes the systematic errors associated with uncertainties in the topological and exclusive D meson decay branching ratios. All C1, C3, C5, V2, V4 and V6 decays were used in this analysis. Impact parameter and decay length cuts were applied to assure good decay visibility and to suppress  $D_s$  and  $\Lambda_c$  decays in the charged charm sample. Table 3 gives these cuts and summarizes the number of accepted decays for each topology. Monte Carlo decay simulations were used to determine the fraction of the D decays removed by the cuts [7]. The cross section is given by:

$$\sigma = \frac{1}{S.B} \sum_{i=1}^3 \frac{N_i \cdot w_i}{\epsilon_i}$$

where the summation is over the three observed topologies,  $N_i$  is the number

of decays surviving the cuts,  $w_i$  the weight which corrects for the loss of events due to the cuts,  $\epsilon_i$  the scanning efficiency, B the branching ratio [ $B(D^\pm \rightarrow C1 + C3 + C5) = 1.0$ ;  $B(D^0 \rightarrow V2 + V4 + V6) = 0.86 \pm 0.04$ ] (see section 4.5) and S is the sensitivity of the experiment. The final data sample consists of 217  $D/\bar{D}$  decays leading to the following cross sections (all  $x_F$ ):

$$\begin{aligned}\sigma(D^+/D^-) &= (11.9 \pm 1.5) \mu\text{b} \\ \sigma(D^0/\bar{D}^0) &= (18.3 \pm 2.5) \mu\text{b} \\ \sigma(D/\bar{D}) &= (30.2 \pm 3.3) \mu\text{b}\end{aligned}$$

The quoted errors include the systematic effects. These sources of uncertainties (sensitivity, weights, branching ratios, scanning efficiency) amount to less than 7% for  $D^+/D^-$  and 9% for  $D^0/\bar{D}^0$ .

At this point it is interesting to mention that the cross section measured in the  $x_F > 0$  hemisphere in pp collisions at 400 GeV/c ( $\sigma(D/\bar{D}) = (15.1 \pm 1.7) \mu\text{b}$ ) is very similar to the one obtained in  $\pi^-p$  interactions at 360 GeV/c ( $\sigma(D/\bar{D}) = (15.8 \pm 2.7) \mu\text{b}$ ) [4], indicating that the dominant underlying mechanism is  $gg \rightarrow c\bar{c}$ , rather than  $q\bar{q} \rightarrow c\bar{c}$ .

We have also calculated the D-meson ( $C = +1$ ) and  $\bar{D}$ -meson ( $C = -1$ ) production cross sections (all  $x_F$ ):

$$\begin{aligned}\sigma(D^0) &= (10.5 \pm 1.9) \mu\text{b} \\ \sigma(\bar{D}^0) &= (7.9 \pm 1.7) \mu\text{b} \\ \sigma(D^+) &= (5.7 \pm 1.1) \mu\text{b} \\ \sigma(D^-) &= (6.2 \pm 1.1) \mu\text{b}\end{aligned}$$

A sample of events with a pair of charm decays was used to measure the cross sections for  $D\bar{D}$  pair production:

$$\begin{aligned}\sigma(D^+D^-) &= (2.5 \pm 0.7) \mu\text{b} \\ \sigma(D^+\bar{D}^0 + D^-\bar{D}^0) &= (6.2 \pm 1.3) \mu\text{b} \\ \sigma(D^0\bar{D}^0) &= (5.9 \pm 1.4) \mu\text{b} \\ \sigma(D\bar{D}) &= (14.6 \pm 2.0) \mu\text{b}\end{aligned}$$

The observation that  $\sigma(D/\bar{D})$  is about twice  $\sigma(D\bar{D})$ , implies that  $D\bar{D}$  pair

production is the dominant source of the  $D/\bar{D}$  mesons and that  $\Lambda_c \bar{D}/\bar{\Lambda}_c D$  associated production is small. Note also that one does not observe an excess of  $\bar{D}$  ( $C = -1$ ) over  $D$  ( $C = +1$ ) production ( $\sigma(\bar{D}) = 14.1 \mu\text{b}$ ,  $\sigma(D) = 16.2 \mu\text{b}$ ), consistent with a small  $\Lambda_c \bar{D}$  cross section (see section 5).

We have also estimated an upper limit for the ratio of two charm pair to one charm pair production by comparing the number of interactions with 1, 2, 3 or 4 associated charm decay candidates and find:

$$\sigma(\text{pp} \rightarrow 4 \text{ charm} + X)/\sigma(\text{pp} \rightarrow 2 \text{ charm} + X) < 1.5\% \text{ at } 90\% \text{ C.L.}$$

A measurement of  $D^*$  production cross sections was made by associating a sample of  $D$  mesons with measured momenta with  $\pi^\pm$  mesons or  $\pi^0$ 's reconstructed from photons measured in the lead glass calorimeters. The  $D\pi$  invariant mass spectra shown in Fig. 5 were used to extract the  $D^*$  signal and the cross sections were calculated using the branching ratios:  $\text{BR}(D^{*+} \rightarrow D^0\pi^+) = 0.49 \pm 0.08$  and  $\text{BR}(D^{*0} \rightarrow D^0\pi^0) = 0.52 \pm 0.08$ . For more details about this calculation see [7]. The measured inclusive  $D^*/\bar{D}^*$  cross sections (all  $x_F$ ) are:

$$\begin{aligned} \sigma(D^{*+}/D^{*-}) &= (9.2 \pm 2.4) \mu\text{b} \\ \sigma(D^{*0}/\bar{D}^{*0}) &= (5.8 \pm 2.7) \mu\text{b} \\ \sigma(D^*/\bar{D}^*) &= (15.0 \pm 3.6) \mu\text{b} \end{aligned}$$

This inclusive  $D^*/\bar{D}^*$  cross section is about half the  $D/\bar{D}$  inclusive cross section, indicating that  $D^*$  decays are an important source of  $D$  mesons.

A large variety of experiments have measured charm production cross sections. The majority, however, used targets heavier than hydrogen. In order to compare the results obtained from interactions on heavy targets one needs to make assumptions on the  $A$  dependence of the charm cross section, a subject which has been treated in [8]. The number of experiments performing charm cross section measurements in  $pp$  interactions is rather limited.

Using a prototype version of the LEBC-EHS set-up exposed to a 360 GeV/c proton beam, the NA16 experiment obtained a cross section of  $\sigma(D/\bar{D}; \text{ all } x_F) = (31.0 \pm \begin{smallmatrix} 16.6 \\ -9.2 \end{smallmatrix}) \mu\text{b}$  at  $\sqrt{s} = 26 \text{ GeV}$  [9], in very good agree-



ment with the results presented in this paper. From an experiment performed at Fermilab with a 800 GeV/c proton beam ( $\sqrt{s} = 38.8$  GeV) and the LEBC bubble chamber, the value  $\sigma(D/\bar{D}; \text{all } x_F) = (51 \begin{smallmatrix} + 16 \\ - 14 \end{smallmatrix}) \mu\text{b}$  was obtained [10].

The other charm production cross section data come from ISR experiments at  $\sqrt{s} = 53$  and 62 GeV. Measurements based on signals in invariant mass plots lead to cross sections of the order of several mb [11], whereas measurements based on the observation of dilepton pairs are of the order of 70  $\mu\text{b}$  [12]. These results, affected by large statistical and systematical uncertainties, only provide a tentative wide range of values for the cross sections.

The inclusive cross section for charm meson production will be discussed in section 7.

#### 4.2 DIFFERENTIAL CROSS SECTIONS

The analysis of the differential distributions is based on 119 decays with fully determined momenta and  $x_F > 0$ . This sample consists of 24  $D^+$ , 27  $D^-$ , 29  $D^0$ , 22  $\bar{D}^0$ , 16  $D^0/\bar{D}^0$  ambiguous and 1  $D^\pm$  ambiguous.

In Fig. 6 we present the measured  $d\sigma/dx_F$  and  $d\sigma/dp_T^2$  spectra for the  $D/\bar{D}$  mesons, corrected for the bubble chamber visibility and spectrometer acceptance efficiencies. The solid curves show the result of a fit to the empirical form:

$$\frac{d^2 \sigma}{dx_F dp_T^2} \propto (1 - |x_F|)^n e^{-bp_T^2}$$

This fit gives  $n = 4.9 \pm 0.5$  and  $b = (0.99 \pm 0.09) (\text{GeV}/c)^{-2}$  (see Table 4) and provides a good description of the measured distributions. There is no need to invoke a two component fit to reproduce the  $x_F$  dependence as was the case with the  $\pi^-$  data [4]. The average values of  $x_F$  and  $p_T$ , for decays having  $x_F > 0$ , are  $\langle |x_F| \rangle = 0.15 \pm 0.02$  and  $\langle p_T \rangle = (0.86 \pm 0.09) \text{ GeV}/c$ . The overall  $x_F$  spectrum is rather central, an observation which can be better quantified by the ratio:

$$\frac{\sigma(D/\bar{D}; x_F > 0.5)}{\sigma(D/\bar{D}; x_F > 0.0)} = 0.02 \begin{array}{l} + 0.02 \\ - 0.01 \end{array}$$

We have also studied separately the distributions for the different D mesons. In Fig. 7 we show the results of fitting the  $x_F$  (non-invariant form,  $(d\sigma/dx_F) \propto (1 - x_F)^n$ ) and the  $p_T^2$  ( $d\sigma/dp_T^2 \propto \exp(-bp_T^2)$ ) distributions. They are also given in table 4, together with the results for fitting to the invariant form  $(1/E) (d\sigma/dx_F) \propto (1 - x_F)^m$  for  $x_F > 0$ . The  $D^-$  and  $D^0$  distributions agree well with each other and are compatible with the distribution of all D's, whereas the  $D^+$  ( $\bar{D}^0$ ) distribution is significantly harder (softer). A possible explanation of this effect, in terms of leading diquark production, has been discussed in [13]. The leading diquark effect would tend to push the D ( $C = +1$ ) mesons ( $D^+$  and  $D^0$ ) towards large  $x_F$  values, leaving the  $\bar{D}$  ( $C = -1$ ) behind. Note that the analysis of the  $D^0$  and  $\bar{D}^0$  is complicated by the existence of the 16  $D^0/\bar{D}^0$  ambiguous decays which show a relatively hard  $x_F$  distribution. Assigning these decays equally to  $D^0$  ( $\bar{D}^0$ ) would bring the  $D^0$  ( $\bar{D}^0$ ) result closer to the  $D^+$  ( $D^-$ ); there remains a significant difference between D and  $\bar{D}$  production, as expected if a diquark effect is present.

#### 4.3 $D\bar{D}$ CORRELATIONS

From the 233 events having a pair of charm candidates we extract two samples: A) pairs where both decays have a clear topological signature and B) fully reconstructed pairs.

Sample A is used to study angular correlations in the transverse plane and sample B, with lesser statistics but more detailed information, is used to investigate  $x_F$ ,  $p_T^2$ , effective mass and the rapidity gap ( $\Delta y$ ) distributions.

The distribution of the angle  $\phi_T$  between two charm hadrons in the plane transverse to the beam direction is shown in Fig. 8 for the 107 events of sample A. The typical error on  $\phi_T$  is of the order of 12 degrees. The dashed histogram represents the raw data. Since these raw data are affected by large errors when the transverse decay length of the charmed particles is small, we introduce the following procedure to correct the  $\phi_T$

distribution. Charm pairs are generated in a Monte Carlo simulation according to the fusion model including LUND fragmentation (see section 7). The positions of the primary and secondary vertices are smeared with gaussian distributions taking the error values from the experiment. The ratio of the  $\phi_T$  distributions before and after smearing gives the correction factor. The solid histogram in Fig. 8 represents the corrected  $\phi_T$  distribution. The forward-backward ratio is  $0.45 \pm 0.09$  and the mean value of the corrected distribution is  $\langle \phi_T \rangle = (114 \pm 5)$  degrees. We also show in this figure the theoretical predictions which we discuss in section 7. We have investigated the ratio of the  $p_T$  of the two charm hadrons making the pair. The average value of this quantity is  $0.61 \pm 0.05$ , similar to the value  $0.55 \pm 0.10$  obtained with the  $\pi^-p$  data. The fusion model calculations are in good agreement with these measurements.

To construct sample B we start with 50 events having kinematic fits for both decays. We then select a set of 17  $D\bar{D}$  pairs produced forward in the c.m.s., each D having a value of  $x_F$  larger than -0.1.

The following weight is applied to every pair

$$w = w_{S_1} \cdot w_{S_2} \cdot w_{amb} \cdot \min(w_{V_1}, w_{V_2})$$

where  $w_S$  and  $w_V$  are the spectrometer and visibility weights of the corresponding decay that take into account the reconstruction and detection losses and  $w_{amb}$  stands for the inverse of the number of accepted fit hypotheses for the given pair. The sum of weights for the 17 events is 45.9.

In Fig. 9 we show the weighted distributions for the effective mass,  $x_F$ ,  $p_T^2$  and rapidity gap of the pairs having positive  $x_F$ . We notice that the  $D\bar{D}$  is preferentially produced at low values of the  $x_F$  variable and that the rapidity gap is fairly small, a reminiscence of short range correlations. Mean values of those quantities are collected in Table 5, where we also include the  $\pi^-p$  data [14]. It is interesting to remark that the spectra obtained in the proton exposure exhibit very similar features to those from the  $\pi^-$  data. The curves in Fig. 9 are theoretical predictions which will be briefly discussed in section 7.

#### 4.4 D MESON LIFETIMES

In an earlier publication [15], we describe 4 different methods that we had used to determine  $D^0$  and  $D^\pm$  lifetimes. These were:

- i) Kinematical fits. The observed lengths and fitted momenta of the D mesons are used to determine the decay times, which are then used in a standard maximum likelihood analysis.
- ii) Momentum estimator [16]. From the observed charged decay tracks (assumed to be pions), an effective mass M and an observed momentum are calculated. By comparing M with the known D mass, we obtain an estimate of the true momentum of the D. This was then incorporated, together with the observed decay length, into a likelihood method to determine the lifetimes.
- iii) Impact parameters [17]. The distances by which the backward extrapolation of the decay tracks miss the production vertex depend on the D lifetimes. The mean impact parameter  $\langle y \rangle$  was used to determine the lifetimes, the relation between  $\langle y \rangle$  and  $\tau$  having been obtained by Monte Carlo calculations.
- iv) Transverse lengths. The transverse distance  $l_T$  of the D decay vertex with respect to the beam direction is related to the decay time of the D meson and to the production transverse momentum by the expression

$$l_T = c \tau p_T/m$$

A knowledge of the  $p_T$  distribution is used to obtain information on the decay times and hence on the D lifetimes.

The advantage of methods (ii) to (iv) is that, since they do not require kinematical fits but only a clear signature that the decay is indeed a  $D^0$  or a  $D^\pm$ , the event sample is larger. This increase in statistics compensates partially for the fact that the D momentum is not precisely known.

In the study reported in [18], we used the method (i) for events which had kinematical fits and the method (iv) for those which did not, having checked that the various techniques gave consistent results. A likelihood function was constructed for each of these two subsamples. The product of these likelihoods was taken as a function of  $\tau$  and its maximum gave an estimate of  $\tau$ . An alternative technique for combining the correlated estimates from the 4 different methods is given in [19].

In this experiment the detection of charm decays relies on the impact parameters of the charged products at the production vertex. This implies that the minimum observable decay length  $l_{\min}$  depends on the decay configuration and on the charm momentum. In our previous work, the method (iv) involved an approximate treatment of  $l_{T,\min}$ . The small bias resulting from the approximation ( $\leq 8\%$ ) was corrected using Monte Carlo calculations.

Recently, to determine the lifetime of charm particles with unknown momenta, we have developed general estimators which make use of the production properties but also include a rigorous treatment of  $l_{\min}$  [20]. We summarize below the basic points of this general analysis, which has been extensively checked by Monte Carlo techniques and which leads to negligible bias and minimum variance estimations. The total error on  $\tau$  does not exceed 1.15 times the error obtained from an equivalent sample of decays with kinematical fits.

The production properties are assumed to be given by the following expression (see section 4.2):

$$\frac{\partial^2 N}{\partial p_T \partial x_F} = \left( 2 b p_T e^{-b p_T^2} \right) \frac{n+1}{2} (1 - |x_F|)^n$$

The joint production and decay distribution is

$$\frac{\partial^3 N}{\partial p_T \partial x_F \partial t} = \frac{\partial^2 N}{\partial p_T \partial x_F} \frac{1}{\tau} e^{-t/\tau}$$

The likelihood function is then

$$L(\tau) = \prod_i \frac{N_i}{D_i}$$

where the numerator is

$$N_i = \left. \frac{\partial^2 N}{\partial \theta \partial l} \right|_i = \int_{p_{\min}}^{p_{\max}} \frac{\partial^3 N}{\partial p \partial \theta \partial l} A(p, \theta) g(p, l) dp \Big|_i$$

in the above,  $\partial^3 N / \partial p \partial \theta \partial l$  is obtained from  $\partial^3 N / \partial p_T \partial x_F \partial t$  by the appropriate Jacobian for the transformation of variables; the decay time is replaced by  $ml/cp$ ;  $p_{\min}$ ,  $p_{\max}$  are the kinematic limits on  $p$  for the given laboratory production angle  $\theta$ ; and  $A(p, \theta)$  is the spectrometer acceptance for  $D$  mesons. To guarantee a correct treatment of  $l_{\min}$ , we also introduce the visibility function  $g(p, l)$  which gives the probability that a decay which occurs at a distance  $l$ , will be detectable from its impact parameters and this, for a given value of  $p$ ; the Monte Carlo calculation of the functional form of  $g(p, l)$  involves the isotropy of the  $D$  decay in its rest frame, and the measured branching ratios of its various possible decay modes. Further details are to be found in [20].

The denominator  $D_i$  in the likelihood function is chosen as a normalising factor for  $N_i$ . It is given by

$$D_i = \int_0^{l_{\max, i}} N_i dl$$

We have applied this method to our proton data and we have obtained the following values:

For the V4 topology

$$\tau(D^0) = (4.2 \begin{smallmatrix} + 1.3 \\ - 1.0 \end{smallmatrix}) \times 10^{-13} \text{ s} \quad (22 \text{ decays})$$

and for the C3 decays:

$$\tau(D^\pm) = (10.4 \begin{smallmatrix} + 1.6 \\ - 1.3 \end{smallmatrix}) \times 10^{-13} \text{ s} \quad (87 \text{ decays})$$

The results are in excellent agreement with the lifetime measurement obtained for the full sample of decays [18]:

$$\tau(D^0) = (4.6 \begin{smallmatrix} + 0.6 \\ - 0.5 \end{smallmatrix}) \times 10^{-13} \text{ s} \quad (145 \text{ decays})$$

$$\tau(D^\pm) = (11.2 \begin{smallmatrix} + 1.4 \\ - 1.1 \end{smallmatrix}) \times 10^{-13} \text{ s} \quad (149 \text{ decays})$$

Although the statistics of the NA27 experiment are not as high as those obtained in more recent experiments (e.g. E691 at Fermilab), the quality of the decays reconstructed (and hence any systematic losses) in NA27 remains unmatched. A careful study has shown that the results are basically insensitive to the exact choice of the cuts being employed. Moreover, the precision of the vertex location is particularly good, typically giving a 2.5  $\mu\text{m}$  error on impact parameters in the film plane and 14  $\mu\text{m}$  in the transverse decay lengths. As a consequence of the quality in the vertex detection, the results coming from NA16 and NA27 have exhibited a consistent pattern since the first values were reported, whilst the world average has fluctuated.

In table 6 we summarize the available measurements of the D lifetimes and of the ratio  $\tau(D^\pm)/\tau(D^0)$  [21].

#### 4.5 D MESON BRANCHING RATIOS

The total sample of charm D mesons, produced in  $\pi^-p$  interactions at 360 GeV/c and pp interactions at 400 GeV/c was used to obtain measurements of branching ratios. The details of the analysis are given in [22] and [23]. We first consider topological branching ratios. For neutral decays, using clear topologies and the  $D^0 \rightarrow 0$ -prong branching ratio ( $B(D^0 \rightarrow 0 \text{ charged}) = 0.14 \pm 0.04$ ) extracted from SPEAR [24], we get:

$$B(D^0 \rightarrow 2 \text{ charged}) = 0.69 \pm 0.04$$

$$B(D^0 \rightarrow 4 \text{ charged}) = 0.17 \pm 0.03$$

$$B(D^0 \rightarrow 6 \text{ charged}) < 0.01 \text{ at } 90\% \text{ C.L.}$$

For charged decays we require that the largest impact parameter be greater than 100  $\mu\text{m}$ . This ensures high detection efficiency for all topo-

gies and reduces the background from shortlived charm particles such as  $\Lambda_c$  or  $D_s$ .

We obtain the following results:

$$B(D^\pm \rightarrow 1 \text{ charged}) = 0.44 \pm 0.09$$

$$B(D^\pm \rightarrow 3 \text{ charged}) = 0.53 \pm 0.09$$

$$B(D^\pm \rightarrow 5 \text{ charged}) = 0.03 \pm 0.01$$

which do not rely on data from other experiments. The quoted errors are only statistical. We estimate the systematic errors to be negligible.

To extract information on the number of decay products in the D-meson sample we used the distribution of maximum transverse momentum of the charged decay products. This distribution depends on the number of unseen neutral decay products, but not on the identity of the products. Hence the full sample of measured D decays can be used without requiring kinematical fits. A maximum likelihood fit to the data using Monte Carlo computed distributions gives a mean decay multiplicity of:

$$3.4 \pm 0.2 \text{ for } D^0 \text{ in V2}$$

$$4.1 \pm 0.2 \text{ for } D^+ \text{ in C3}$$

$$4.6 \begin{array}{l} + 0.2 \\ - 0.1 \end{array} \text{ for } D^0 \text{ in V4}$$

The errors include uncertainties due to final state interactions, like  $\rho$  and  $K^*$  resonances, as well as the presence of semileptonic decays.

A maximum likelihood method, which uses the ISIS ionization measurement for the charged particles, allows the determination of the charged kaon and electron content of the charm decay tracks [22]. Results are shown in Table 7 for the different decay topologies. Combining these results with the quoted topological branching ratios, we get the following inclusive ratios for the D-meson into charged kaons:

$$B(D^\pm \rightarrow K^\mp + \text{anything}) = 0.17 \pm 0.07$$

$$B(D^\pm \rightarrow K^\pm + \text{anything}) = 0.08 \begin{array}{l} + 0.06 \\ - 0.05 \end{array}$$

$$B(D^0 \rightarrow K^\pm + \text{anything}) = 0.42 \pm 0.08$$



$$B(D^0 \rightarrow K^+ + \text{anything}) = 0.03 \begin{array}{l} + 0.05 \\ - 0.02 \end{array}$$

and the following semielectronic branching ratios:

$$B(D^0 \rightarrow e^\pm + \text{anything}) = 0.15 \pm 0.05$$

$$B(D^\pm \rightarrow e^\pm + \text{anything}) = 0.20 \begin{array}{l} + 0.09 \\ - 0.07 \end{array}$$

The  $D^0$ ,  $D^+$  ratios into charged kaons and the  $D^+$  semielectronic ratio are in agreement with the world average [25]. The result for the  $D^0$  semielectronic ratio is somewhat unexpected in view of the value  $0.075 \pm 0.011 \pm 0.004$  published in [26]. Evidence for semi-leptonic decays other than  $D \rightarrow K_{\text{ev}}, K^*_{\text{ev}}$  follows from the observation of the  $V_4$  semileptonic decay given in Table 7. Our results are based on modest statistics but have negligible systematic errors.

In this experiment 9 D meson decays give unique fits to Cabibbo unfavoured modes ( $D_{\text{un}}$ ), which include all-pion decays as well as wrong sign kaons. From the inclusive branching ratios into a charged kaon plus anything, given above, a total of 4.3 decays having a "wrong sign" kaon (i.e., a kaon corresponding to a Cabibbo unfavoured solution) is expected in the sample of D decays with unique fits. We have observed 4 such decays.

Some exclusive branching ratios of the D-mesons have also been determined. The detailed analysis is described in [23]. We first consider exclusive branching ratios to all charged final states for  $D^0$  and  $D^+$ . We require a unique 3C kinematical fit. For the decay modes involving neutral products we used a different approach not related to kinematical fits. We evaluated the quantity  $M^2$  defined in section 3.3. The value of this quantity allows a statistical discrimination between decays with one or more neutral products. The results are shown in Table 8. They are in good agreement with those obtained by the MARK III collaboration [26] on the same final states.

The available samples of neutral and charged decays fully reconstructed do not warrant a statistically meaningful investigation, which was nevertheless tried, of the existence of final state interactions among their decay products.

#### 4.6 GENERAL FEATURES OF CHARM EVENTS

The large acceptance and the high multitrack efficiency achieved in this experiment allow a study of the complete final states and extraction of some general properties of the hadronic charm production processes. In what follows we briefly describe how the overall charged multiplicity and the event shape are influenced by the presence of charm. A more detailed analysis will be published elsewhere [27].

The measurement of the multiplicity requires a topological signature for the charm decay. In this analysis all charged hadrons produced at the primary vertex, including charm particles, were considered but charged decay products were not counted. By using only events for which both charm particles are identified biases, due to undetected charm were excluded. The average charged multiplicity for the charm sample was  $11.0 \pm 0.5$ , whereas the multiplicity derived from the non charm data was  $8.98 \pm 0.01$  (these values have been corrected for losses induced by the interaction trigger used in this experiment).

The significance of the measured difference may be quantified by noticing that an increase of the beam momentum from 400 GeV/c up to 1060 GeV/c would be required to produce a rise of  $\langle n \rangle$  from 8.98 to 11.0 in soft pp interactions [28]. The observed increase in the value of the mean charged multiplicity underlines the central character of hadronic charm production at this energy.

Information on the event shape for final states with charm content was obtained by analysing the quantity  $1 - \langle T \rangle$ , where the thrust T was defined as

$$T = \max (\Sigma p_{\parallel} / \Sigma p)$$

The quantity T was calculated, in terms of charged tracks only, for the 101 events having, at least, one charm particle and more than one charged non charm track emitted in the forward c.m.s. hemisphere. Corrections

were made to account for visibility and acceptance losses and kinematical ambiguities. An average value of  $1 - \langle T \rangle = 0.12 \pm 0.01$  was obtained. The investigation of the event shape shows that  $1 - \langle T \rangle$  increases with increasing multiplicity of the final state, a behaviour approximately reproduced by the QCD fusion model with hard fragmentation. On the other hand, it is found that final states with charm are much broader than final states without charm.

## 5. $\Lambda_c$ BARYON DECAY AND PRODUCTION PROPERTIES

Seven non-ambiguous  $\Lambda_c/\bar{\Lambda}_c$  have been observed in this experiment (proton run). They have been extracted from 67 C3 decays with three well reconstructed tracks. To define these non-ambiguous  $\Lambda_c/\bar{\Lambda}_c$  we require the presence of a uniquely identified proton (antiproton) among the decay products with the same charge as the parent particle (like-sign) or a C3 kinematical fit without any other fits to  $D^\pm$  or  $D_s$ .

A "unique" proton is defined by an ISIS mass assignment probability larger than 1% and at least 10 times the probability obtained for K or  $\pi$  mass assignment. For high momentum tracks the Forward Cerenkov information is used to reject mass assignments with probability smaller than 5%.

The seven  $\Lambda_c$  are presented in Table 9. Events 1, 2 and 3 have  $\Lambda_c$  fits with a unique proton identified. Events 4 to 7 have one 3C  $\Lambda_c$  fit with no competing hypothesis compatible with particle identification.

Combining this sample with the three non-ambiguous  $\Lambda_c/\bar{\Lambda}_c$  observed in  $\pi^-p$  interactions [4], we find through a maximum likelihood analysis a lifetime of [29]:

$$\tau(\Lambda_c) = (1.2 \begin{smallmatrix} + 0.5 \\ - 0.3 \end{smallmatrix}) \times 10^{-13} \text{ s} \quad (9 \text{ decays})$$

which is significantly smaller than the lifetimes measured for the  $D^0$  and the  $D^\pm$  in this experiment.

Several experiments have measured the  $\Lambda_c$  lifetime [30]. Within the errors these measurements are in agreement and seem to indicate a lifetime

in the range  $(1-2) \times 10^{-13}$  s (see Table 10).

Among the 10  $\Lambda_c/\bar{\Lambda}_c$  shown in Table 9 one notes that five of them have a  $pK\pi$  decay mode. To determine the mass of the  $\Lambda_c$ , we have investigated the effective mass ( $pK\pi$  hypothesis) of all the C3 decays with three well reconstructed tracks and having an average impact parameter,  $\langle y \rangle$ , smaller than  $60 \mu\text{m}$ . This cut enhances the  $\Lambda_c$  signal, since its lifetime is small compared to the  $D^\pm$  one, which is the main background. In the  $\Lambda_c$  mass bin (Fig. 10), we find six entries, five of them having a unique 3C fit to the  $pK\pi$  decay mode. The value of the  $\Lambda_c$  mass using these five events is:

$$M(\Lambda_c) = (2284.7 \pm 2.3 \pm 0.5) \text{ MeV}/c^2$$

where the first error is statistical and the second systematic.

Available data on the mass of the  $\Lambda_c$  cluster around two different values ( $\sim 2260$  and  $2285 \text{ MeV}/c^2$ ) [25], [31], as shown in Table 11. Their global compatibility is not very good ( $\chi^2 = 44$  for 17 measurements). The subset of data using the  $pK\pi$  decay mode is statistically consistent. The average of this sample,  $M(\Lambda_c) = (2285.40 \pm 0.88) \text{ MeV}/c^2$ , is in very good agreement with our measurement.

To determine the  $\Lambda_c/\bar{\Lambda}_c$  cross section three different, but complementary, methods have been applied. They are based on the impact parameter distribution, the proton identification among the decay products and the kinematical fits. The results given in [32] can be summarized as follows.

The inclusive  $\Lambda_c/\bar{\Lambda}_c$  production cross section times the topological branching ratio  $B(\Lambda_c \rightarrow 3 \text{ charged})$  is, for all  $x_F$ , in the range:

$$1.4 \mu\text{b} < \sigma(\Lambda_c/\bar{\Lambda}_c) \cdot B(\Lambda_c \rightarrow 3 \text{ charged}) < 6.1 \mu\text{b} \quad \text{at } 90\% \text{ C.L.}$$

The inclusive  $\Lambda_c/\bar{\Lambda}_c$  production cross section times the branching ratio  $B(\Lambda_c \rightarrow pK\pi)$  is:

$$\sigma(\Lambda_c/\bar{\Lambda}_c) \cdot B(\Lambda_c \rightarrow pK\pi) = (1.2 \begin{matrix} + 1.6 \\ - 0.8 \end{matrix}) \mu\text{b}$$

From the single  $D$ ,  $\bar{D}$  and  $D\bar{D}$  pair production cross sections and the ratio  $\sigma(\Lambda_c \bar{\Lambda}_c)/\sigma(\Lambda_c \bar{D}/\bar{\Lambda}_c D)$  the following limits on the associated production

$\Lambda_c \bar{D}/\bar{\Lambda}_c D$  and on the inclusive  $\Lambda_c/\bar{\Lambda}_c$  production are obtained

$$\sigma(\Lambda_c \bar{D}/\bar{\Lambda}_c D) < 6.1 \text{ } \mu\text{b at 90\% C.L.}$$

$$\sigma(\Lambda_c/\bar{\Lambda}_c) < 15 \text{ } \mu\text{b at 95\% C.L.}$$

the  $\Lambda_c$  and  $\bar{\Lambda}_c$  inclusive cross sections being of the same order.

Since these cross sections have been calculated using visibility weights computed from the value of the lifetime measured in this experiment, we must indicate that a change in the lifetime by one standard deviation will modify the quoted values by 25-40% (i.e., the cross sections should be increased by 40% if  $\tau(\Lambda_c) = 0.9 \times 10^{-13}$  s and decreased by 25% if  $\tau(\Lambda_c) = 1.7 \times 10^{-13}$  s).

Using the 5 uniquely identified  $\Lambda_c/\bar{\Lambda}_c$  with positive  $x_F$  (decays 1-5 in Table 9) the following mean values for  $x_F$  and  $p_T^2$  are calculated:

$$\langle |x_F(\Lambda_c/\bar{\Lambda}_c)| \rangle = 0.13 \pm 0.05$$

$$\langle |x_F(\Lambda_c)| \rangle = 0.17 \pm 0.06$$

$$\langle |x_F(\bar{\Lambda}_c)| \rangle = 0.08 \pm 0.07$$

$$\langle p_T(\Lambda_c/\bar{\Lambda}_c) \rangle = (1.15 \pm 0.34) \text{ GeV/c}$$

From the cross section values given above we have made the following branching ratio estimation

$$B(\Lambda_c \rightarrow pK\pi) > 4.4\% \quad \text{at 90\% C.L.}$$

This limit decreases by 20% assuming a lifetime of  $1.7 \times 10^{-13}$  s (instead of  $1.2 \times 10^{-13}$  s).

## 6. $D_s$ MESON STUDY

For the study of  $D_s$  mesons two independent sets of selection criteria have been applied to the C3 and C5 samples.

The first method, similar to the one used for the  $\Lambda_c$  with uniquely identified protons, relies on the detection of a charged K meson, among the decay products, having the same sign as the parent charm particle. Only two known types of charm decays can lead to this configuration: the  $D_S^\pm \rightarrow K^\pm + X$  and the Cabibbo unfavoured  $D_{un}^\pm \rightarrow K^\pm + X$  decays. When applying this method, a charged K is considered to be uniquely identified if its ISIS probability is at least ten times larger than the pion one. The response of the FC is also taken into account. Two non-ambiguous  $D_S^\pm$  have been found in this way (events 1 and 2 of Table 12). One also finds two non-ambiguous  $D_{un}^\pm$  decays.

The other method applies the standard selection procedure explained in section 3.3. Among the 38 decays having a  $D_S^\pm$  fit, 20 are ambiguous with Cabibbo favoured  $D^\pm$  decays, 14 are ambiguous with  $D_{un}^\pm$  decays and the 4 decays listed in table 12 (they include the two  $D_S^\pm$  selected by the first method) give only a  $D_S^\pm$  interpretation. For some of the 14 ambiguous  $D_S/D_{un}$  decays, the  $\Lambda_c$  hypothesis cannot be excluded.

Before discussing the properties of the  $D_S$  sample, the events containing the unique  $D_S$  are described in some detail (see Table 12):

Event 1: The pp interaction leads to a charged multiplicity of 14. The  $\pi^-$  hypothesis for the  $K^-$  track is ruled out by particle identification. The 3C fit for the  $D_S$  is preferred over a 0C solution for a  $D^-$  (Cabibbo unfavoured). The charm partner has an unclear decay topology. There is an additional ( $K^+/p$ ) at the primary vertex and a further  $K^-$ , which could belong to the second decay, suggesting that a  $D_S^- D_S^+$  or a  $D_S^- D^+ K^+$  could be present in the final state.

Event 2: The charged primary multiplicity is 10. The C5 and the C3 are topologically well defined charm decays. The only kinematical possibility is a  $D_S$  2C fit, which is strongly favoured by particle identification. Its partner (a C3) can be either a  $D_S$  or a  $D/\Lambda_c$ . This ambiguity cannot be resolved although the particle identification prefers the  $D_S/\Lambda_c$  solutions.

Event 3: It has 14 charged tracks at the primary vertex and two good charm decays. The only kinematical solution is a 2C fit for the  $D_S$ . Both

kaons are allowed by particle identification but the pion hypothesis is not excluded. However, the effective mass of the  $K^+K^-$  system ( $1017 \text{ MeV}/c^2$ ) indicates a decay mode in  $\phi\pi\pi$ . Its partner (a C1) gives multineutral fits to  $D/D_S/\Lambda_c$ .

Event 4: The charged primary multiplicity is 8 including two clearly visible charm decays (C3). The only kinematical hypothesis is a  $D_S$  decay into four pions. No  $\phi$  nor  $\eta$  can be constructed from the decay particles. The muon hypothesis for all 3 decay tracks is excluded by the hadron calorimeters as well as the electron hypothesis by the electromagnetic calorimeters. Its partner is a  $D^+$  meson decaying semileptonically.

Concerning the production properties one might note the central production of the  $D_S$  mesons; the mean value of the Feynman  $x$  distribution is  $\langle |x_F| \rangle = 0.05 \pm 0.10$ . The average  $p_T$  is equal to  $(0.88 \pm 0.45) \text{ GeV}/c$ .

The estimated lifetime obtained by a maximum likelihood analysis with the four decays is  $(7.7^{+6.8}_{-3.0}) \times 10^{-13} \text{ s}$  and is compatible, within one standard deviation, with the world average  $(4.33^{+0.41}_{-0.32}) \times 10^{-13} \text{ s}$  [30]. Our value is affected by the long lifetime of the last decay. Removing this decay the mean lifetime value is  $(4.5^{+4.0}_{-2.0}) \times 10^{-13} \text{ s}$ .

The 14  $D_S^\pm/D_{un}^\pm$  ambiguous decays can be distributed, statistically, between the  $D_S^\pm$  and  $D_{un}^\pm$  population in the ratio of the non ambiguous  $D_S^\pm$  to  $D_{un}^\pm$ , which is 4/4; this distribution is in agreement with the average lifetime measured for the 14  $D_S^\pm/D_{un}^\pm$  ( $\tau = (6.6^{+2.8}_{-1.7}) \times 10^{-13} \text{ s}$ ), which is consistent for an equal mixture of  $D_S^\pm$  and  $D_{un}^\pm$ . In the same way, the 20  $D_S^\pm/D_{un}^\pm$  can be distributed in the ratio of the number of non-ambiguous  $D_S^\pm$  to  $D_{un}^\pm$  which has the value 4/32.

In summary, one can estimate that the sample of 38 decays contains 13  $D_S^\pm$ , 11  $D_{un}^\pm$  and 14  $D^\pm$ . Using a sensitivity of 38.5 events/ $\mu\text{b}$  and a detection efficiency of 95%, one obtains (all  $x_F$ ):

$$\sigma(D_S) \times B(D_S \rightarrow 3 \text{ and } 5 \text{ charged}) = (0.7 \pm 0.4) \mu\text{b}$$

We estimate that the background of  $D_S$  decays in the sample of  $D^\pm$  decays used for the determination of the inclusive cross sections is below 10%.

Assuming a value of 50% for the branching ratio  $B(D_S \rightarrow 3 \text{ and } 5 \text{ charged})$  an upper limit of 2.5  $\mu\text{b}$  (at 90% C.L.) is derived for the overall  $D_S$  cross section for all  $x_F$ .

## 7. COMPARISON OF CHARM PRODUCTION TO THE QCD FUSION MODEL

The QCD fusion model can be used to calculate the D meson production spectrum. The calculation requires: 1) a description of the parton content of the proton, 2) a calculation of the cross sections for the subprocesses  $gg \rightarrow c\bar{c}$  and  $qq \rightarrow c\bar{c}$  and 3) some approximation for the  $c \rightarrow D$  fragmentation process. Since the predictions of the model depend on the detailed treatment of the above components, we have allowed some variation of the input parameters. For a description of the parton content of the proton we used the structure functions determined by Duke and Owens (DO) [33] and Eichten et al. (EHLQ) [34]. The intrinsic parton transverse momentum plus soft gluon radiation effects were included by giving the colliding partons a transverse momentum,  $k_T$ , with a distribution  $dN/dk_T^2 = \exp(-k_T^2/\langle k_T^2 \rangle)/\langle k_T^2 \rangle$ . Since the main production mechanism is  $gg \rightarrow c\bar{c}$ , this is the  $\langle k_T^2 \rangle$  for gluons, as opposed to that for quarks as measured in, for example, Drell-Yan processes. The parameter  $\langle k_T^2 \rangle$  was allowed to vary between 0 and  $0.64 \text{ (GeV/c)}^2$  [35], although it can be directly calculated from the  $p_T^2$  distribution of the  $D\bar{D}$  hadroproduced system,  $\langle k_T \rangle = [(\pi/8) \langle p_T^2_{D\bar{D}} \rangle]^{1/2}$  [36]. The subprocess parton cross sections have been derived by Combridge [37]. For the  $c\bar{c}$  production threshold we use  $(2m_c)^2$ , where the charm quark mass is allowed to vary from 1.2 to 1.4  $\text{GeV/c}^2$ . The strong interaction coupling constant is given by  $\alpha_s = (12\pi/25)/\log(Q^2/\Lambda^2)$  where  $\Lambda$  is taken to be 0.2  $\text{GeV}$  and  $Q^2$  is allowed to vary between  $(2m_c)^2$  and  $\hat{s}$ , the cm energy squared of the subprocess. Finally we have investigated the sensitivity of the D meson differential production cross section to two different  $c \rightarrow D$  fragmentation processes: 1) a  $\delta$ -function in which all the longitudinal momentum of the charm quark is transferred to the D meson (dashed curves in Figs. 8, 9 and 11), and 2) a fragmentation which approximates the final state  $c\bar{q}$  and  $\bar{c}q$  formation via



colour string breaking as described by the Lund model [38] (solid curves in Figs. 8, 9 and 11). The last depends on adjustable string parameters but these were not changed from the values determined by the Lund group. It has been shown in the analysis of the  $\pi^-p$  data [14] that the distributions (in particular the  $p_T^2$  and the rapidity gap of the  $D\bar{D}$  pair) cannot be explained in terms of the Peterson fragmentation function [39]. This is also true for the pp data and we do not show the corresponding predictions.

Comparison of some predictions of this QCD fusion model, normalized to our data, are shown in Figs. 8, 9 and 11. The shape of the calculated  $x_F$  and  $p_T^2$  distributions are relatively insensitive to the choice of structure functions and charm quark mass. The curves shown on the figures were obtained using the EHLQ set 1 structure functions and a charm quark mass of 1.25 GeV/c<sup>2</sup>. The  $d\sigma/dp_T^2$  distribution is sensitive to the effective parton intrinsic  $k_T$  and the QCD prediction with  $\langle k_T^2 \rangle = 0$  does not fit the data. The value  $\langle k_T^2 \rangle = 0.64$  (GeV/c)<sup>2</sup> was used to produce the theoretical curves in Fig. 11b. This value is similar to the one determined in Drell-Yan processes and from the analysis of  $D\bar{D}$  pairs produced in our experiment ( $\langle k_T \rangle = (0.7 \pm 0.1)$  GeV/c from 400 GeV/c pp data,  $\langle k_T \rangle = (0.8 \pm 0.1)$  GeV/c from 360 GeV/c  $\pi^-p$  data [14], [36]).

The dashed curve in Figs. 8, 9 and 11 is the fusion model prediction with inputs fixed as described in the above paragraph and using a  $\delta$ -function  $c \rightarrow D$  fragmentation. This illustrates the basic parton level prediction. If the isolated  $c \rightarrow D$  fragmentation of Peterson et al. [39] is added to the calculation, the predicted momentum spectrum is too soft and disagrees with both the measured  $d\sigma/dx_F$  and  $d\sigma/dp_T^2$  spectra. The Lund  $c \rightarrow D$  fragmentation process is sensitive to the production environment of the  $c\bar{c}$  pair, since colour singlet strings are formed between the charm quarks and the valence quarks and diquarks left over from the proton after the hard scattering process. The predictions of this calculation [38] are given by the solid curves shown in Figs. 8, 9 and 11. The fusion model plus Lund fragmentation clearly reproduces well the measured  $x_F$  and  $p_T^2$  distributions of the total sample of  $D/\bar{D}$  mesons. However, a closer examination of the predictions indicates some discrepancies between the model and our data. In particular, the fusion/Lund model does not predict our observation (section 4.2) that the D mesons have a somewhat flatter  $x_F$  spectrum than the  $\bar{D}$  mesons.

The same QCD fusion model with Lund fragmentation reproduces rather well (see Figs. 8 and 9) the main features of the  $D\bar{D}$  correlation variables: namely  $\phi_T$ , effective mass,  $x_F$ ,  $\Delta y$  of the  $D\bar{D}$  pairs and  $p_T^2$  as long as we introduce an intrinsic transverse momentum of the initial partons with  $\langle k_T^2 \rangle = 0.64 \text{ (GeV/c)}^2$ .

A comparison of the measured  $D/\bar{D}$  inclusive cross section,  $\sigma(D/\bar{D})$ , to the predictions of QCD is difficult. The problem is that the fusion model calculation is inherently uncertain for several reasons. First, the subprocess cross sections for  $gg \rightarrow c\bar{c}$  and  $qq \rightarrow c\bar{c}$  are very sensitive to the threshold determined by the charm quark mass [40]. For example, if  $m_c$  is varied between 1.2 and 1.4 GeV/c<sup>2</sup>, the cross section for  $pp \rightarrow c\bar{c} + X$  varies by a factor 2.2. Additional factors of almost 2 arise from changing the proton structure functions. Smaller variations in the cross section come from the choice of  $Q^2$  in  $\alpha_s$  and the evolution of the structure functions. Also, in order to calculate  $pp \rightarrow D/\bar{D} + X$ , an estimate of the fraction of  $c(\bar{c})$  quarks producing  $D(\bar{D})$  mesons must be made. Using the Lund fragmentation scheme as a guide, the ratio  $\sigma(pp \rightarrow D/\bar{D} + X)/\sigma(pp \rightarrow c/\bar{c} + X)$  is found to be 0.8. Data obtained in  $e^+e^-$  reactions give a value of  $\sim 0.8$  for the  $D(\bar{D})$  over  $c(\bar{c})$  fraction [41]. In summary, the  $D/\bar{D}$  cross section calculated from the fusion model has a large uncertainty. Nonetheless, we can calculate the ratio of our measured  $D/\bar{D}$  inclusive cross section to the fusion model prediction in order to obtain a rough estimate of the  $O(\alpha_s^2)$  corrections to charm hadroproduction cross sections. The ratio is:

$$k = [\sigma(pp \rightarrow D/\bar{D} + X)]/[0.8 \sigma(pp \rightarrow c/\bar{c} + X)] = 1.2 \text{ to } 2.7$$

where the range corresponds to a change of the charm quark mass from 1.2 to 1.4 GeV/c<sup>2</sup>. We have used for this calculation the EHLQ set one structure functions and  $(2m_c)^2$  as  $\hat{s}$  threshold. Our data indicate that the charm  $k$ -factor is of the order of 2 with a large error caused by uncertainties in the fusion model calculation (basically in the charm quark mass). A discussion of the  $k$  factor in charm hadroproduction is given in [41]. A comparison of this measurement to the fusion model calculations including higher order  $O(\alpha_s^3)$  corrections [42] will test the capability of QCD to predict the detailed behaviour of charm hadroproduction.

## 8. CONCLUSIONS

In this paper we have summarized the most significant results obtained in an experiment designed to study the decay and production properties of charm particles produced in pp interactions at 400 GeV/c.

The experiment has been performed in the LEBC-EHS complex at the CERN SPS and relies on the highly effective capability of optically detecting the production and decay vertices of shortlived particles produced in a liquid hydrogen target. A large acceptance spectrometer with good momentum resolution and adequate particle identification assures a high reconstruction efficiency for the decay products of charm particles and permits the extraction of samples with only small systematic errors. The strength of the experimental technique used in this work is best quantified by the fact that approximately 50% of all the charm particles produced in the forward hemisphere have been observed, the detection efficiency being a smooth function of the kinematical variables  $x_F$  and  $p_T^2$ . This remarkable detection capability leads to small and well understood correction factors, allowing the determination of charm particle decay and production properties.

From the study of 1,015,000 interactions in the hydrogen target ( $38.5 \pm 1.1$  events/ $\mu\text{b}$ ) we have isolated 324 events containing 557 charm decays. In a previous exposure of LEBC to an incident  $\pi^-$  beam of 360 GeV/c (265,000 interactions,  $15.8 \pm 0.8$  events/ $\mu\text{b}$ ), 114 charm events with 183 decays were collected. They have been added to the sample reported in this paper for the measurement of some intrinsic properties of charm hadrons.

The most relevant results obtained in this work are:

1. The measurement of the following inclusive total cross sections for single D production in the full  $x_F$  range

$$\sigma(\text{pp} \rightarrow \text{D}^0 + \text{X}) = (10.5 \pm 1.9) \mu\text{b}$$

$$\sigma(\text{pp} \rightarrow \bar{\text{D}}^0 + \text{X}) = (7.9 \pm 1.7) \mu\text{b}$$

$$\sigma(\text{pp} \rightarrow \text{D}^+ + \text{X}) = (5.7 \pm 1.1) \mu\text{b}$$

$$\sigma(pp \rightarrow D^- + X) = (6.2 \pm 1.1) \mu\text{b}$$

$$\sigma(pp \rightarrow D^+/D^- + X) = (11.9 \pm 1.5) \mu\text{b}$$

$$\sigma(pp \rightarrow D^0/\bar{D}^0 + X) = (18.3 \pm 2.5) \mu\text{b}$$

$$\sigma(pp \rightarrow D/\bar{D} + X) = (30.2 \pm 3.3) \mu\text{b}$$

These measurements have been obtained using free nucleon targets and are therefore not affected by any A dependent effects.

2. The measurement of the following inclusive total cross sections for  $D\bar{D}$  pair production

$$\sigma(pp \rightarrow D^+D^- + X) = (2.5 \pm 0.7) \mu\text{b}$$

$$\sigma(pp \rightarrow D^+\bar{D}^0 + D^-D^0 + X) = (6.2 \pm 1.3) \mu\text{b}$$

$$\sigma(pp \rightarrow D^0\bar{D}^0 + X) = (5.9 \pm 1.4) \mu\text{b}$$

$$\sigma(pp \rightarrow D\bar{D} + X) = (14.6 \pm 2.0) \mu\text{b}$$

The ratio of the single D to the  $D\bar{D}$  pair production cross sections indicates a small  $\Lambda_c \bar{D}$  cross section compared to  $D\bar{D}$ .

3. The measurement of the following inclusive total cross sections for  $D^*$  ( $2010$ ) production

$$\sigma(pp \rightarrow D^{*+}/D^{*-} + X) = (9.2 \pm 2.4) \mu\text{b}$$

$$\sigma(pp \rightarrow D^{*0}/\bar{D}^{*0} + X) = (5.8 \pm 2.7) \mu\text{b}$$

$$\sigma(pp \rightarrow D^*/\bar{D}^* + X) = (15.0 \pm 3.6) \mu\text{b}$$

$D^*$  decays are an important source of D meson production.

4. The measurement of the following multicharm production rate

$$\sigma(pp \rightarrow 4 \text{ charm} + X) / \sigma(pp \rightarrow 2 \text{ charm} + X) < 1.5\% \quad \text{at } 90\% \text{ C.L.}$$

5. The measurement of the longitudinal and transverse inclusive differential cross sections for all the D states. Although the overall shape of the inclusive distribution for all D's can be reproduced by the fusion model with the Lund fragmentation, there appear to be some differences among the production spectra for the various states. Qualitatively the observed pattern can be explained in terms of leading diquark production. The transverse distributions can be described in the context of the fusion model requiring a value of  $\langle k_T^2 \rangle$  equal to  $0.64 \text{ (GeV/c)}^2$ .
6. The measurement of  $x_F$ ,  $p_T^2$ ,  $M_{D\bar{D}}$ ,  $\Delta y$ ,  $\phi_T$  for pairs of charm meson decays. The observed distributions can be qualitatively described by the fusion model.
7. Using samples of 145  $D^0/\bar{D}^0$  decays and of 149  $D^+/D^-$  decays we have measured the following values for the neutral and charged charm particle lifetimes

$$\tau(D^0/\bar{D}^0) = (4.6 \begin{smallmatrix} + 0.6 \\ - 0.5 \end{smallmatrix}) \times 10^{-13} \text{ s}$$

$$\tau(D^+/D^-) = (11.2 \begin{smallmatrix} + 1.4 \\ - 1.1 \end{smallmatrix}) \times 10^{-13} \text{ s}$$

8. The measurement of the following topological and inclusive branching ratios

$$B(D^0 \rightarrow 2 \text{ charged}) = 0.69 \pm 0.04$$

$$B(D^0 \rightarrow 4 \text{ charged}) = 0.17 \pm 0.03$$

$$B(D^0 \rightarrow 6 \text{ charged}) < 0.01 \quad \text{at } 90\% \text{ C.L.}$$

$$B(D^\pm \rightarrow 1 \text{ charged}) = 0.44 \pm 0.09$$

$$B(D^\pm \rightarrow 3 \text{ charged}) = 0.53 \pm 0.09$$

$$B(D^\pm \rightarrow 5 \text{ charged}) = 0.03 \pm 0.01$$

$$B(D^\pm \rightarrow K^\mp + X) = 0.17 \pm 0.07$$

$$B(D^\pm \rightarrow K^\pm + X) = 0.08 \begin{matrix} + 0.06 \\ - 0.05 \end{matrix}$$

$$B(D^0 \rightarrow K^\pm + X) = 0.42 \pm 0.08$$

$$B(D^0 \rightarrow e^\pm + X) = 0.15 \pm 0.05$$

$$B(D^+ \rightarrow e^+ + X) = 0.20 \begin{matrix} + 0.09 \\ - 0.07 \end{matrix}$$

and some exclusive branching ratios.

9. We have used a sample of 9 (10) non-ambiguous  $\Lambda_c/\bar{\Lambda}_c$  baryon decays to measure the following value of the lifetime (mass)

$$\tau(\Lambda_c) = (1.2 \begin{matrix} + 0.5 \\ - 0.3 \end{matrix}) \times 10^{-13} \text{ s}$$

$$M(\Lambda_c) = (2284.7 \pm 2.3 \pm 0.5) \text{ MeV}/c^2$$

10. The measurement of the following values of products of  $\Lambda_c/\bar{\Lambda}_c$  cross section times branching ratios

$$1.4 \text{ } \mu\text{b} < \sigma(pp \rightarrow \bar{\Lambda}_c/\Lambda_c + X) \cdot B(\Lambda_c \rightarrow 3 \text{ charged}) < 6.1 \text{ } \mu\text{b} \quad \text{at } 90\% \text{ C.L.}$$

$$\sigma(pp \rightarrow \Lambda_c/\bar{\Lambda}_c + X) \cdot B(\Lambda_c \rightarrow pK\pi) = (1.2 \begin{matrix} + 1.6 \\ - 0.8 \end{matrix}) \text{ } \mu\text{b}$$

and the mean values of  $|x_F|$  ( $\langle |x_F(\Lambda_c)| \rangle = 0.17 \pm 0.06$ ,  $\langle |x_F(\bar{\Lambda}_c)| \rangle = 0.08 \pm 0.07$ ) and  $p_T$  ( $\langle p_T(\Lambda_c/\bar{\Lambda}_c) \rangle = (1.15 \pm 0.34) \text{ GeV}/c$ ). In this experiment no evidence was found for a dominant  $\Lambda_c$  production at large  $x_F$ .

11. We have estimated the cross sections for  $D_S$  decaying into 3 or 5 prongs to be

$$\sigma(pp \rightarrow D_S^\pm + X) B(D_S^\pm \rightarrow 3 \text{ and } 5 \text{ charged}) = (0.7 \pm 0.4) \text{ } \mu\text{b}$$

The mean  $x_F$  value for  $D_S$  is  $0.05 \pm 0.10$ , to be compared with  $0.15 \pm 0.02$  obtained for the D sample. The averaged  $p_T$  is similar for  $D_S$  and D production ( $(0.88 \pm 0.45)$  GeV/c and  $(0.86 \pm 0.09)$  GeV/c, respectively).

#### ACKNOWLEDGEMENTS

We are indebted to the CERN staff, whose sterling performance was essential in collecting the data for this experiment. We also would like to take the opportunity to acknowledge the heroic effort by our scan and measurement personnel. Financial assistance by various national funding agencies is gratefully acknowledged.

REFERENCES

- [1] M. Aguilar-Benitez et al., Nucl. Instrum. and Meths. 205 (1983) 79  
M. Aguilar-Benitez et al., Phys. Lett. 122B (1983) 312
- [2] M. Aguilar-Benitez et al., Phys. Lett. 123B (1983) 98  
M. Aguilar-Benitez et al., Phys. Lett. 123B (1983) 103
- [3] M. Aguilar-Benitez et al., Phys. Lett. 135B (1984) 237
- [4] M. Aguilar-Benitez et al., Z. Phys. C 31 (1986) 491
- [5] M. Aguilar-Benitez et al., Nucl. Instr. and Meths. A258 (1987) 26
- [6] J.R. Lutz and A. Michalon: II Vezelay Workshop on EHS,  
CERN/EP-EHS/PH 80-2
- [7] M. Aguilar-Benitez et al., Phys. Lett. 189B (1987) 476
- [8] S. Reucroft and M. MacDermott, Phys. Lett. 184B (1987) 108
- [9] M. Aguilar-Benitez et al., Phys. Lett. 123B (1983) 98  
M. Aguilar-Benitez et al., Phys. Lett. 135B (1984) 237
- [10] R. Ammar et al., Phys. Lett. 183B (1987) 110
- [11] A. Putzer, "Results on Charm Production", Contrib. to the Int.  
Europhys. Conf. on HEP, Brighton (July 1983) 308-309  
W.M. Geist, "Strangeness, charm and beauty production at the Split  
Field Magnet detector", Talk at the 2<sup>nd</sup> Moriond Workshop on New  
Flavours (1982)
- [12] A. Chilingarov et al., Nucl. Phys. B151 (1979) 29  
A. Chilingarov et al., Phys. Lett. 83B (1979) 136  
A. Clark et al., Phys. Lett. 77B (1978) 339
- [13] M. Aguilar-Benitez et al., Phys. Lett. 201B (1988) 176



- [14] M. Aguilar-Benitez et al., Phys. Lett. 164B (1985) 404.
- [15] M. Aguilar-Benitez et al., Z. Phys. C 34 (1987) 143
- [16] B. Franek, Rutherford Preprint, RAL 85-026  
"A production model independent calculation of charmed particle lifetime using unconstrained decays"
- [17] A.G. Carlson, J.E. Hooper and D.T. King, Phil. Mag. 41 (1950) 701  
S. Petrera and G. Romano, Nucl. Inst. and Meths. 174 (1980) 61
- [18] M. Aguilar-Benitez et al., Phys. Lett. 193B (1987) 140
- [19] L. Lyons, D. Gibaut and P. Clifford, Oxford preprint 5/88  
"How to combine correlated estimates of a single physical quantity"
- [20] NA27 Collaboration, "Estimation of the lifetime of shortlived particles from their production characteristics" (in preparation)
- [21] a) H. Fuchi et al., Lett. Nuov. Cim. 31 (1981) 199  
b) E. Albinì et al., Phys. Lett. 110B (1982) 339  
c) M. Aguilar-Benitez et al., Phys. Lett. 122B (1983) 312  
d) A. Badertscher et al., Phys. Lett. 123B (1983) 471  
e) R. Bailey et al., Z. Phys. C 28 (1985) 357  
f) H. Yamamoto et al., Phys. Rev. D 32 (1985) 2901  
g) K. Abe et al., Phys. Rev. D 33 (1986) 1  
h) N. Ushida et al., Phys. Rev. Lett. 56 (1986) 1767  
N. Ushida et al., Phys. Rev. Lett. 56 (1986) 1771  
i) M. Althoff et al., Z. Phys. C 34 (1986) 343  
j) L. Gladney et al., Phys. Rev. D 34 (1986) 2601  
k) J.C. Anjos et al., Phys. Rev. Lett. 58 (1987) 311  
l) M. Adamovich et al., Europhys. Lett. 4 (1987) 887.  
m) S.R. Wagner et al., Phys. Rev. D 36 (1987) 2850  
n) S.E. Csorna et al., Phys. Lett. 191B (1987) 318  
p) S. Barlag et al., Z. Phys. C 37 (1987) 17  
r) R.M. Baltrusaitis et al., Phys. Rev. Lett. 54 (1985) 1976.

- [22] M. Aguilar-Benitez et al., Z. Phys. C 36 (1987) 551
- [23] M. Aguilar-Benitez et al., Z. Phys. C 36 (1987) 559
- [24] G. H. Trilling, Phys. Rep. 75 (1981) 57  
I. Peruzzi et al., Phys. Rev. Lett. 39 (1977) 1301  
R. Schindler et al., Phys. Rev. D24 (1984) 78
- [25] Review of Particle Properties, Phys. Lett. 170B (1986) 1
- [26] R.M. Baltrusaitis et al., see [21]
- [27] M. Aguilar-Benitez et al., General Features of Charm Production in pp Interactions at 400 GeV/c; to be published in Z. Phys. C
- [28] A. Breakstone et al., Phys. Rev. D30 (1984) 528
- [29] M. Aguilar-Benitez et al., Phys. Lett. 189B (1987) 254
- [30] D. Hitlin, Talk presented at the 1987 Int. Symp. on Lepton and Photon Int. at High Energies, Hamburg (July 1987)
  - a) N. Ushida et al., see [21]
  - b) L. Cremaldi, Contrib. to the APS Meeting on Particles and Fields, Salt Lake City, Utah (January 1987).
  - c) S. Barlag et al., Phys. Lett. 184B (1987) 283
  - d) M. Adamovich et al., see [21]
  - f) S.R. Amendolia et al., Z. Phys. C 36 (1987) 513
- [31]
  - a) E.G. Cazzoli et al., Phys. Rev. Lett. 34 (1975) 1125
  - b) B. Knapp et al., Phys. Rev. Lett. 37 (1976) 882
  - c) A.M. Cnops et al., Phys. Rev. Lett. 42 (1979) 197
  - d) C. Baltay et al., Phys. Rev. Lett. 42 (1979) 1721
  - e) K.L. Giboni et al., Phys. Lett. 85B (1979) 437
  - f) G.S. Abrams et al., Phys. Rev. Lett. 44 (1980) 10
  - g) D. Allasia et al., Nucl. Phys. 176B (1980) 13
  - h) M. Calicchio et al., Phys. Lett. 93B (1980) 521
  - i) T. Kitagaki et al., Phys. Rev. Lett. 45 (1980) 955
  - j) J.J. Russell et al., Phys. Rev. Lett. 46 (1981) 799

- k) P.C. Bosseti et al., Phys. Lett. 109B (1981) 234
  - l) T. Kitagaki et al., Phys. Rev. Lett. 48 (1982) 299
  - m) A.N. Aleev et al., Z. Phys. C 23 (1984) 333
  - n) N. Ushida et al., see [21]
  - p) M. Adamovich et al., see [21]
  - q) S. Barlag et al., see [30]
- 
- [32] M. Aguilar-Benitez et al., Phys. Lett. 199B (1987) 462
  - [33] D.W. Duke and J.F. Owens, Phys. Rev. D30 (1984) 49
  - [34] E. Eichten et al., Rev. Mod. Phys. 56 (1984) 667
  - [35] B. Cox and P.K. Malhotra, Phys. Rev. D29 (1984) 63
  - [36] S.N. Ganguli, TIFR-EHEP-87-5
  - [37] B.L. Combridge, Nucl. Phys. B151 (1979) 429
  - [38] H.U. Bengtsson, "CHARIS-The Lund Monte Carlo for Charm Production"  
(private communication)  
H.U. Bengtsson and G. Ingelman, Comp. Phys. Commun. 34 (1985) 231
  - [39] C. Peterson et al., Phys. Rev. D27 (1983) 105
  - [40] J.F. Cudell, F. Halzen and K. Hikasa, Phys. Lett. 175B (1986) 227  
S. Banerjee and S.N. Ganguli, Phys. Rev. D33 (1986) 1278  
K. Ellis, 21<sup>st</sup> Rencontre de Moriond, Ed. Frontieres M50 (1988)  
331.
  - [41] S.N. Ganguli, TIFR-EHEP-87-7
  - [42] K.R. Ellis, Contrib. to the Advanced Research Workshop on QCD Hard  
Hadronic Processes, St. Croix, Virgin Islands (October 1987)

## TABLES

Table 1 Measurement selection criteria. The decay topologies are defined in Section 3.1.

Table 2 Performance of particle identification devices.

Table 3 Cuts applied to select the charm decays for the  $D/\bar{D}$  total cross section calculations.

Table 4 Result of the fits to the invariant and non-invariant differential cross sections for the different D meson states.

Table 5 Mean values of physical quantities measured for  $D\bar{D}$  pairs in 400 GeV/c pp and 360 GeV/c  $\pi^-p$  interactions and model predictions.

Table 6 a) Summary of available measurements of the  $D^0$  lifetimes.  
b) Summary of available measurements of the  $D^\pm$  lifetimes.  
c) Summary of available measurements of the ratio  $\tau(D^\pm)/\tau(D^0)$ .

Table 7 Electron, kaon and proton contents extracted from the information provided by ISIS through a method of maximum likelihood.

Table 8 Exclusive branching ratios of the neutral and charged D. The first error is statistical, the second one is systematic.

Table 9 Unambiguous  $\Lambda_c/\bar{\Lambda}_c$  decays produced in pp and  $\pi^-p$  interactions. A double underlining means a well identified solution, single underlining means the solution is allowed by particle identification but not preferred and no underlining means no particle identification. ( $\pi^0$ ) means that the  $\pi^0$  has not been detected in the electromagnetic calorimeters.

Table 10 Summary of available measurements of the  $\Lambda_c$  lifetimes.

Table 11 Summary of available measurements of the  $\Lambda_c$  mass.

Table 12  $D_s$  candidates. A double underlining means a well identified solution, single underlining means the solution is allowed by particle identification but not preferred, and no underlining means no particle identification. The notation  $(\pi^+)$ ,  $(\pi^-)$  means that the momentum of the charged track has not been measured.

Table 1

Topology	R(mm)	L(cm)	T(mm)	N
X1-X6	2.0	-	1.5	2
C1	0.6	-	1.5	1
V2	0.2	3	0.5	2
C3,V4,C5	2.0	-	-	-

Table 2

	SAD	ISIS	FC	TRD(a)	ALL
Acceptance					
all tracks	0.23	0.84	0.58	0.86	0.87
from charm	0.23	0.82	0.59	-	0.86
Figure of merit					
all tracks	0.66	0.78	0.75	0.68	0.97
from charm	0.70	0.80	0.80	-	0.96
Momentum range (GeV/c)	0.6-3.8	2-50	18-112	70-400	0.6-400

(a) For TRD the quoted numbers refer to tracks with  $p > 70$  GeV, which make up 30% of all tracks in D4 (see fig. 1). Among the charm decay products, this fraction is only 12% and the statistics are very low (12 tracks)

Table 3

Cuts applied to select the charm decays used for the  $D/\bar{D}$  total cross section calculations.

Decay channel	Decay surviving all cuts N (D) i	Decay length (mm)		Transverse length (mm)	Minimum impact parameter lower limit ( $\mu\text{m}$ )	Maximum impact parameter range ( $\mu\text{m}$ )
		Lower limit	Upper limit			
C1	39	2	90	0.6		100-1500
C3	74	1		2.0	20	100-2000
C5	6	1		2.0	20	100-2000
V2	67	2	30	0.2	20	60- 500
V4	30	1		2.0	20	60-1500
V6	1	1		2.0	20	60-1500



Table 4

	Number of decays	n	m	$\langle p_T^2 \rangle$ (GeV/c) <sup>2</sup>
All D	119	4.9±0.5	3.2±0.6	0.99±0.09
D <sup>+</sup>	24	3.1±0.8	1.8±0.7	1.32±0.27
D <sup>-</sup>	27	5.4±1.2	3.5±0.9	1.04±0.20
D <sup>0</sup>	29	5.5±1.2	3.8±0.9	0.82±0.14
D <sup>0</sup> <sub>amb</sub>	22	8.1±1.9	6.2±1.4	0.62±0.14
D <sub>amb</sub>	17	3.9±1.1	2.9±0.9	0.93±0.30
[D <sup>+</sup> + D <sup>0</sup> ]	53	4.2±0.8	2.7±0.6	1.04±0.14
[D <sup>-</sup> + D <sup>0</sup> ]	49	6.6±1.1	4.6±0.8	0.84±0.12

Table 5

	$\langle M(D\bar{D}) \rangle$	$\langle x_F(D\bar{D}) \rangle$	$\langle p_T^2(D\bar{D}) \rangle$	$\langle \Delta y \rangle$	$\langle \phi_T \rangle$
pp-Data (this work)	$4.65 \pm 0.13$	$0.18 \pm 0.03$	$1.50 \pm 0.30$	$1.02 \pm 0.12$	$105 \pm 5$
$\pi^-$ -p-Data [14]	$4.50 \pm 0.16$	$0.25 \pm 0.07$	$1.65 \pm 0.40$	$0.80 \pm 0.14$	$115 \pm 8$
Fusion Model with $\delta$ -fragmentation					
pp-Data	4.63	0.16	1.2	0.69	125
$\pi^-$ -p-Data	4.81	0.23	1.2	0.76	129
LUND-fragmentation					
pp-Data	4.82	0.19	0.88	0.98	119
$\pi^-$ -p-Data	4.60	0.25	0.75	0.77	126

Table 6(a)

D<sup>0</sup> MESON LIFETIME MEASUREMENTS

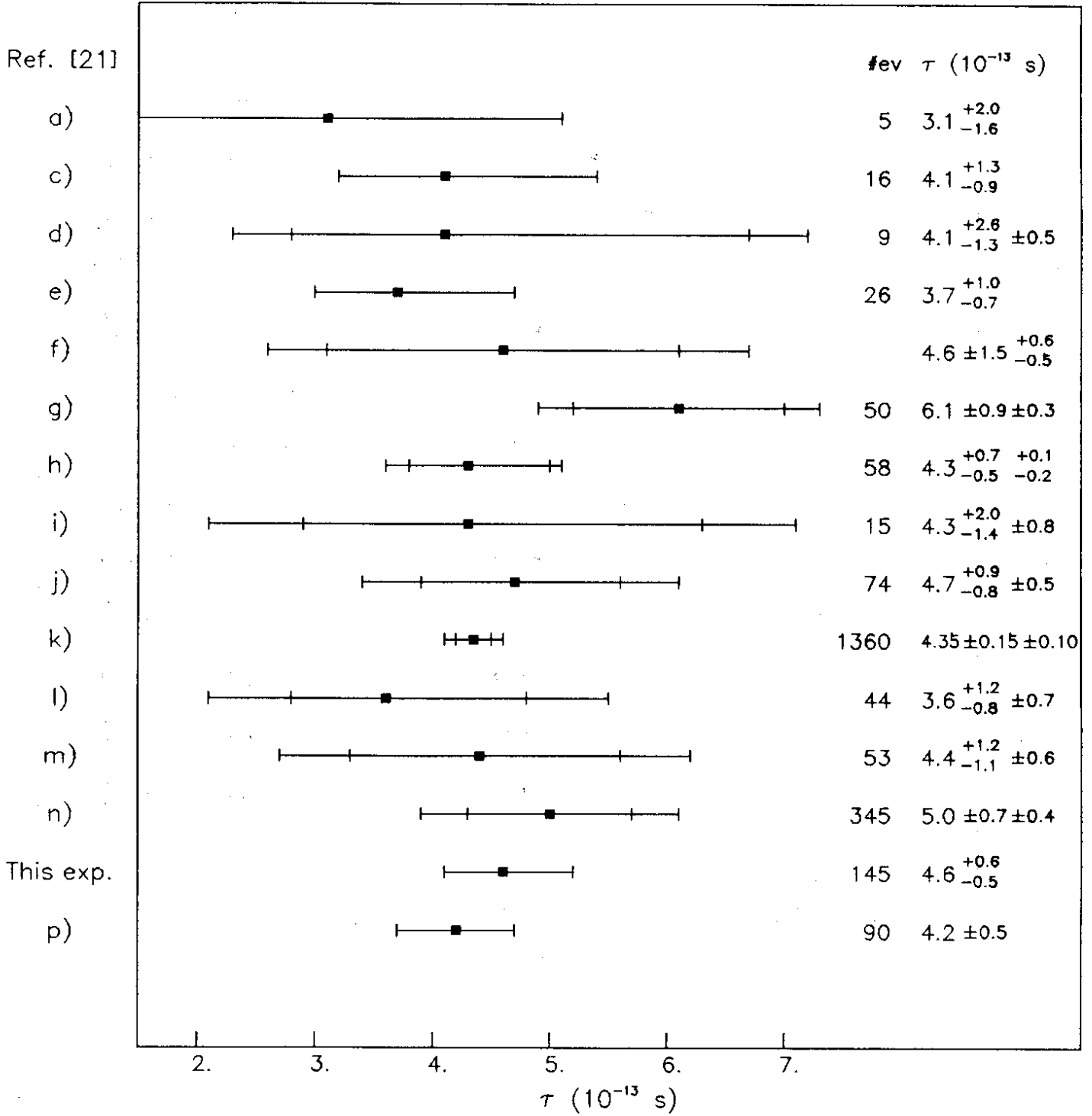


Table 6(b)

$D^{\pm}$  MESON LIFETIME MEASUREMENTS

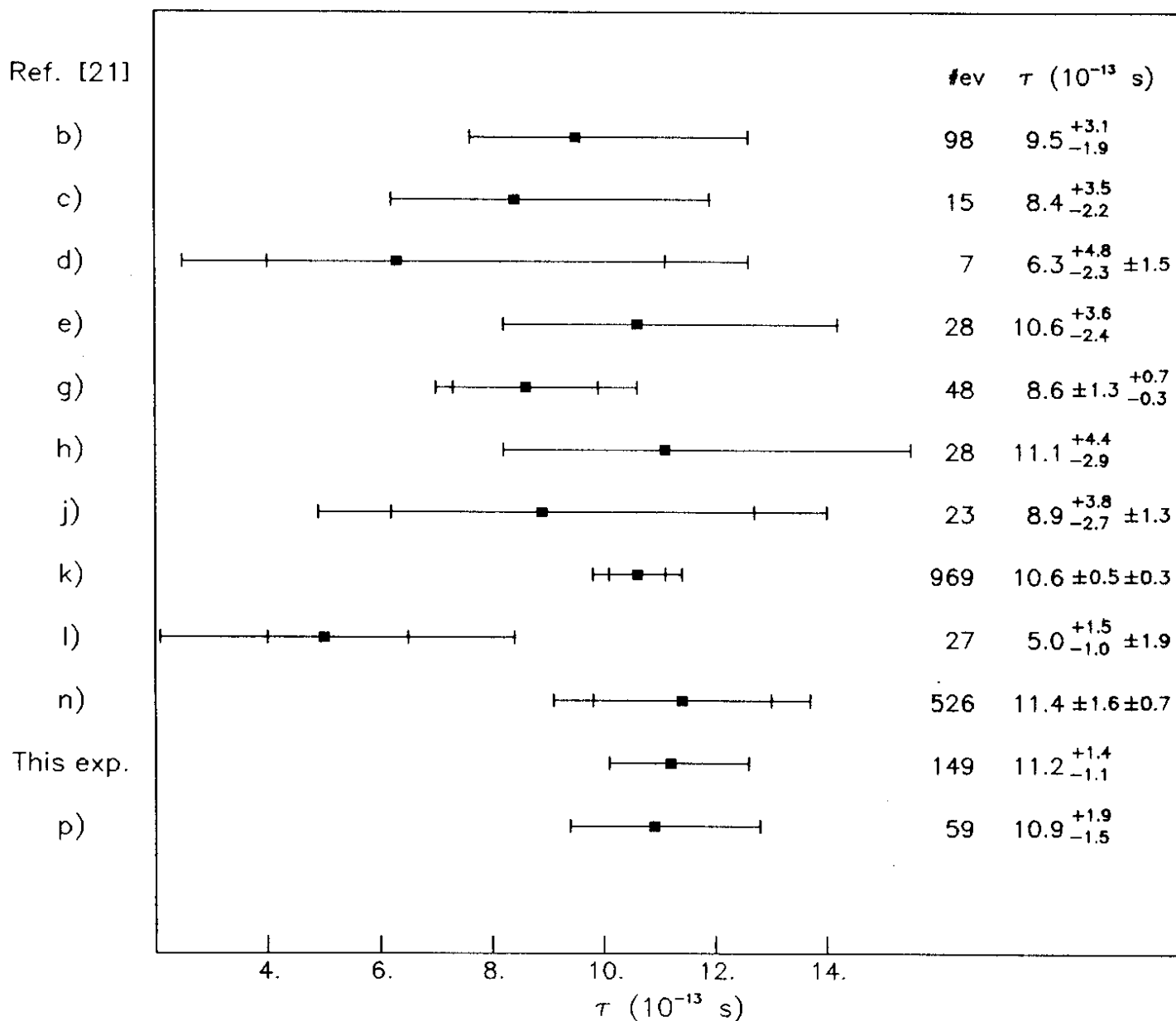


Table 6(c)

MEAN LIFETIME RATIO

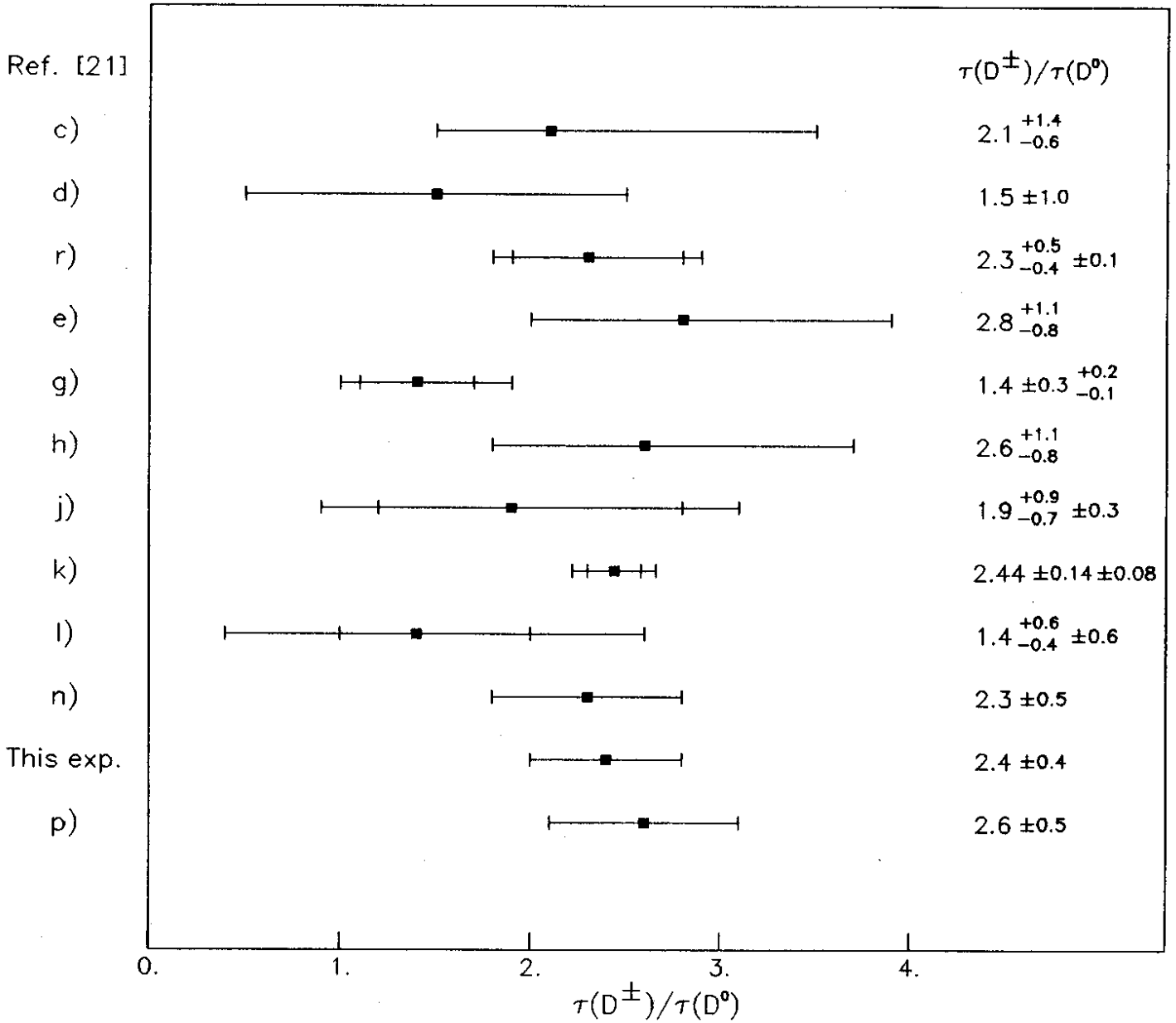


Table 7

Topology of vertices	Number of decay vertices	Fraction tracks with ionization information	Most likely number of:		
			protons	kaons	electrons
C1	23	23/23	( $<5.3$ ) -	$4.4^{+3.0}_{-2.3}$	$5.8^{+3.1}_{-2.5}$
V2	84	134/168	( $<5.3$ ) -	$34.1^{+7.3}_{-6.6}$	$12.7^{+4.7}_{-3.9}$
C3	60	Likesign 85/120	( $<3.0$ ) -	( $<3.7$ ) -	$4.9^{+3.6}_{-2.4}$
		Unlikesign 34/60	( $<3.3$ ) -	$12.3^{+4.6}_{-4.3}$	( $<2.7$ ) -
V4	51	140/204	( $<8.9$ ) -	$22.3^{+6.9}_{-7.0}$	( $<4.9$ ) $1.0^1$
C5	7	Likesign 13/21	( $<2.1$ ) -	( $<2.6$ ) -	( $<2.7$ ) -
		Unlikesign 6/14	( $<4.0$ ) $1.0^2$	( $<3.4$ ) -	( $<3.1$ ) -
V6	1	4/6	( $<2.5$ ) -	( $<4.4$ ) -	( $<1.9$ ) -

The figures shown in brackets correspond to 90% C.L. and blank entries (-) imply that the value preferred by the likelihood function is zero.

<sup>1</sup> There is one electron identified by the lead-glass detectors and supported but not required by ionization. This has been inserted by hand.

<sup>2</sup> The likelihood function prefers this result rather than zero with a likelihood ratio of 1.9 to 1.

Table 8

$D^0 \rightarrow$	B.R.(%)	$D^+ \rightarrow$	B.R.(%)
$K^- \pi^+$	$4.0^{+2.1}_{-1.0} \pm 0.2$	$K^- \pi^+ \pi^+$	$6.3^{+2.8}_{-1.4} \pm 1.1$
$\pi^- \pi^+$	$0.5^{+1.2}_{-0.2} \pm 0.04$	$K^- K^+ \pi^+$	$0.8^{+1.7}_{-0.2} \pm 0.1$
$K^- \pi^+ \pi^0$	$10.6^{+6.1}_{-2.8} \pm 0.6$	$K^- \pi^+ \pi^- \pi^0$	$2.2^{+4.7}_{-0.6} \pm 0.4$
$\bar{K}^0 \pi^+ \pi^-$	$4.5^{+5.9}_{-1.4} \pm 0.3$	$\bar{K}^0 \pi^- \pi^+ \pi^-$	$24.3^{+6.4}_{-4.1} \pm 4.1$
$K^- \pi^+ \pi^+ \geq 2\pi^0$	$20.9^{+7.4}_{-4.3} \pm 1.2$	$K^- \pi^+ \pi^+ \pi^0 \pi^0$	$2.2^{+4.7}_{-0.6} \pm 0.4$
$\bar{K}^0 \pi^- \pi^+ \pi^+ \geq 1\pi^0$	$10.6^{+7.3}_{-2.9} \pm 0.6$	$\bar{K}^0 \pi^- \pi^+ \pi^+ \pi^0$	$4.4^{+5.2}_{-1.3} \pm 0.7$
$K^- \pi^- \pi^+ \pi^+$	$6.5^{+1.7}_{-1.1} \pm 1.9$	$K^- \pi^+ e^+ \nu_e$	$< 5.7^*$
$\pi^- \pi^- \pi^+ \pi^+$	$0.5^{+1.1}_{-0.1} \pm 0.1$	$K^- \pi^+ e^+ \nu_e \pi^0$	$4.4^{+5.2}_{-1.3} \pm 0.7$
$K^- e^+ \nu_e$	$< 5.0^*$	$\pi^- \pi^+ e^+ \nu_e$	$< 5.7^*$
$K^- e^+ \nu_e \pi^+ \geq 2\pi^0$	$2.3^{+5.0}_{-0.6} \pm 0.1$	$\bar{K}^0 \pi^- \pi^+ e^+ \nu_e$	$2.2^{+4.7}_{-0.6} \pm 0.4$
$\pi^- e^+ \nu_e$	$< 5.4^*$		
$\bar{K}^0 \pi^- e^+ \nu_e + 0, 1\pi^0$	$7.9^{+6.9}_{-2.3} \pm 0.5$		

\* 90% C.L. upper limit

Table 9

	id	ndf	Mode	m ( $\Delta m$ ) (MeV/c <sup>2</sup> )	t (10 <sup>-13</sup> s)	t <sub>min</sub> (10 <sup>-13</sup> s)	y <sub>max</sub> ( $\mu m$ )	Partner
pp Data	1	3	$\underline{p}\underline{\pi}^+\underline{\pi}^-\underline{K}^0\underline{\pi}^0$	2307 (35)	0.50	0.57	11	$\bar{D}^0$
	2	3	$\underline{p}\underline{\pi}^+\underline{K}^-\underline{\pi}^0$	2255 (10)	2.96	0.64	83	$D^-$
	3	0	$\underline{p}\underline{K}^+\underline{\pi}^-(\pi^0)$		1.64	0.50	42	$C3^+$
	4	3	$\underline{p}\underline{K}^-\underline{\pi}^+$	2293 (8)	0.82	0.66	62	$C1^-$
	5	3	$\underline{p}\underline{K}^+\underline{\pi}^-$	2295 (5)	1.12	0.61	18	$D^0$
	6	3	$\underline{p}\underline{K}^+\underline{\pi}^-$	2290 (6)	2.57	1.87	68	$D^0$
	7	3	$\underline{p}\underline{K}^-\underline{\pi}^-\underline{\pi}^0$	2309 (14)	5.88	1.55	139	V2
$\pi^-p$ Data	1	3	$\underline{\pi}^+\underline{\pi}^-\underline{\pi}^-\underline{\Lambda}$	2291 (6)	1.25	1.12	55	-
	2	3	$\underline{K}^+\underline{\pi}^-\underline{p}$	2275 (4)	1.93	1.30	32	$D^+$
	3	3	$\underline{K}^-\underline{\pi}^+\underline{p}$	2284 (5)	2.87	1.99	67	X2



Table 10

$\Lambda_c$  BARYON LIFETIME MEASUREMENTS

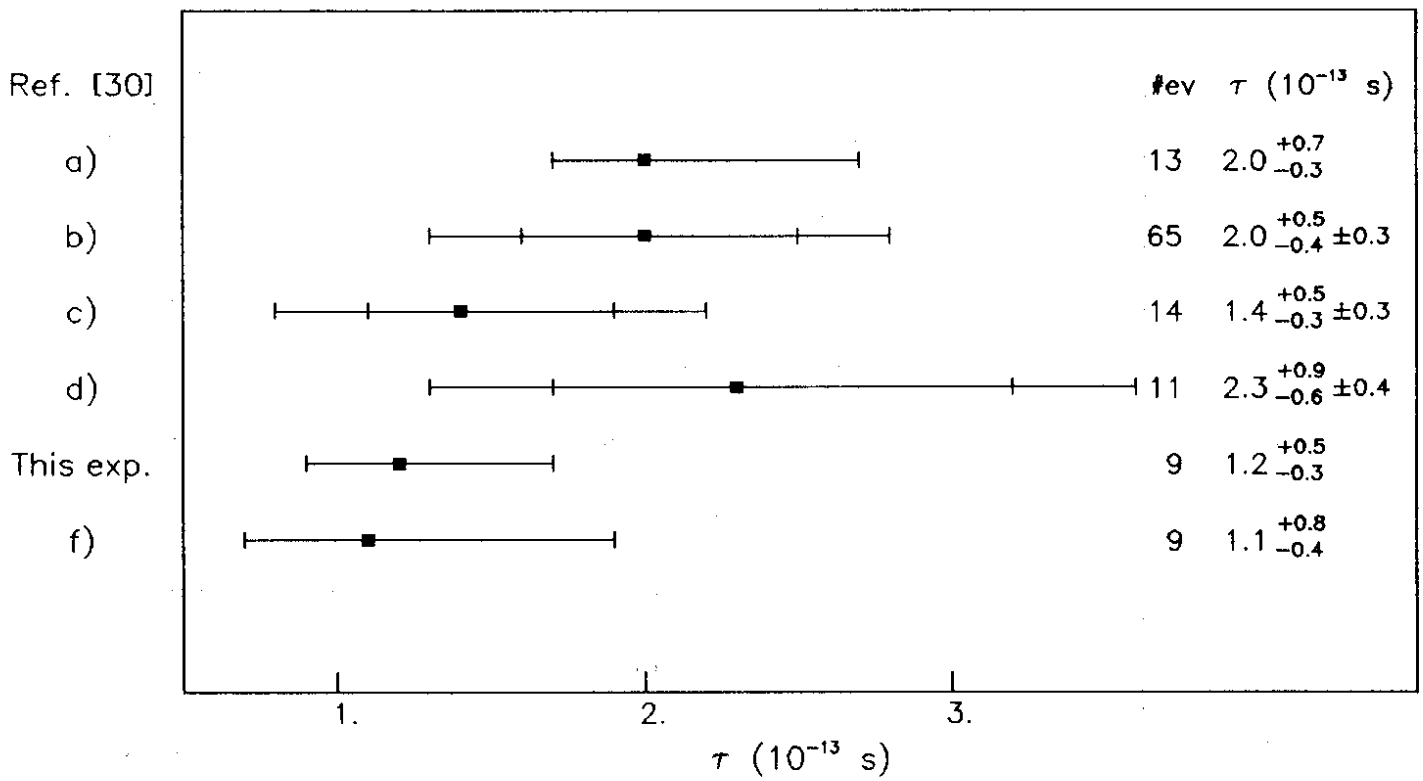


Table 11

$\Lambda_c$  BARYON MASS MEASUREMENTS

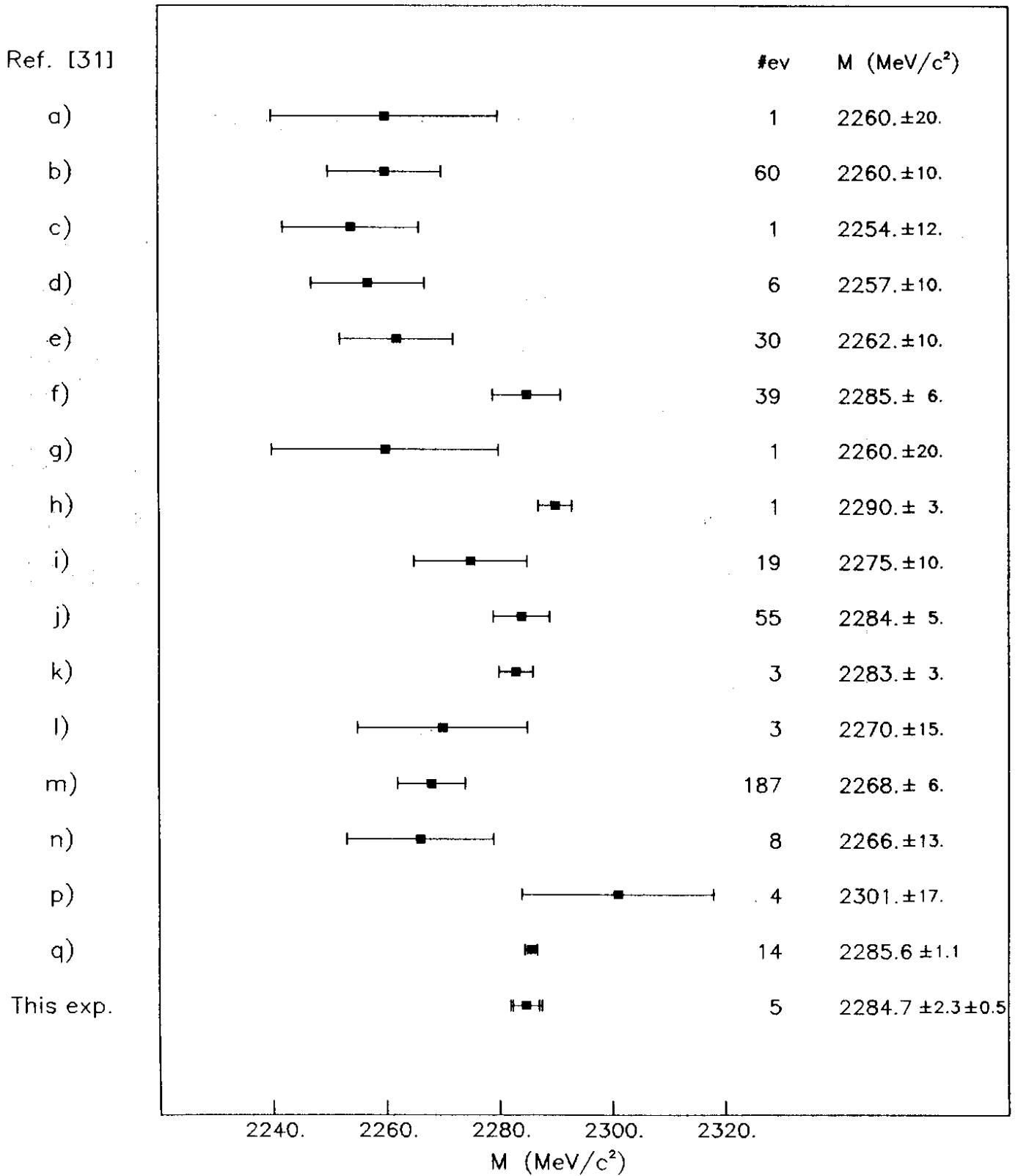


Table 12

Event decay	$x_F$	$p_T$ (GeV/c)	$t$ ( $10^{-13}$ s)	$t_{\min}$ ( $10^{-13}$ s)	$y_{\max}$ ( $\mu\text{m}$ )	Partner
1 $K^+ \underline{\underline{\pi^-}} \underline{\underline{K^-}} \pi^0$	0.000	0.593	5.98	4.02	94	X1
2 $\underline{\underline{K^+}} (\pi^+) \underline{\underline{\pi^-}} \underline{\underline{\pi^-}} \underline{\underline{K^-}}$	-0.048	1.918	4.22	0.78	269	C3
3 $\underline{\underline{K^+}} \underline{\underline{\pi^+}} (\pi^-) \underline{\underline{K^-}} \underline{\underline{\pi^-}}$	-0.061	1.273	9.15	1.16	429	C1
4 $\underline{\underline{\pi^+}} \underline{\underline{\pi^-}} \underline{\underline{\pi^-}} \pi^0$	0.231	0.346	16.43	1.39	593	C3

FIGURE CAPTIONS

Fig. 1 The European Hybrid Spectrometer in the version used for the NA27 proton exposure.

Fig. 2 A V4-V2 event observed in the high resolution bubble chamber LEBC. The picture shows a display of the HPD digitisings of bubble centres with the scale expanded in the transverse direction.

Fig. 3 a) Definition of impact parameter,  $y = L \sin\phi$ .  
 b) definition of the "scan box". Each event was scanned for secondary activity inside the dashed line, a rectangle of width  $\pm 2$  mm centered on the interacting beam. Also shown is the definition of L and  $\theta$ .

Fig. 4 Spectrometer acceptance for neutral D mesons giving three constrained fits. The full line is for decays without neutral particles, the broken line with one observed  $\pi^0$ .

Fig. 5 (a) The  $D^0\pi^\pm$  effective mass spectra from kinematically constrained  $D^0$ 's.  
 (b) The  $D^0\pi^0$  effective mass spectra.  
 Background estimations are given by the broken line.

Fig. 6 (a)  $d\sigma/dx_F$  and (b)  $d\sigma/dp_T^2$  distributions for  $D/\bar{D}$  meson production from pp interactions at  $\sqrt{s} = 27.4$  GeV. The solid curves are fits to the data using distributions of the form

$$\frac{d\sigma}{dx_F} \propto (1 - x_F)^n \quad \text{and} \quad \frac{d\sigma}{dp_T^2} \propto e^{-bp_T^2}$$

The fits determine  $n = 4.9 \pm 0.5$  and  $b = (0.99 \pm 0.09) (\text{GeV}/c)^{-2}$

Fig. 7 Differential cross sections in  $x_F$  and  $p_T^2$  for  $D^+$ ,  $D^0$ ,  $D^-$  and  $\bar{D}^0$  mesons. The solid curves correspond to fits of the form:

$$\frac{d\sigma}{dx_F} \propto (1 - x_F)^n \quad \text{and} \quad \frac{d\sigma}{dp_T^2} \propto e^{-bp_T^2}$$

Fig. 8 Distribution of events as a function of the angle in the transverse plane,  $\phi_T$ , between charm particles for the 107 geometrically reconstructed pairs. The solid histogram represents the corrected experimental distribution, raw data are shown as a dashed histogram. The dashed curve shows the basic parton level prediction ( $\delta$ -function  $c \rightarrow D$  fragmentation) and the solid curve includes fragmentation effects as simulated by coloured string breaking (the Lund model).

Fig. 9  $D\bar{D}$  correlations for 17 fully reconstructed pairs.  
a) Effective mass distribution  
b)  $x_F$  distribution  
c)  $p_T^2$  distribution  
d) rapidity gap,  $\Delta y$ , distribution

The dashed curve shows the basic parton level prediction ( $\delta$ -function  $c \rightarrow D$  fragmentation) and the solid curve includes fragmentation effects as simulated by coloured string breaking (the Lund model).

Fig. 10  $pK\pi$  invariant mass for the C3 decays with an average impact parameter,  $\langle y \rangle$ , smaller than 60  $\mu\text{m}$ .

Fig. 11 Comparisons of the measured inclusive  $D/\bar{D}$   $d\sigma/dx_F$  and  $d\sigma/dp_T^2$  distributions to the fusion model calculation described in the text. The dashed curve shows the basic parton level prediction ( $\delta$ -function  $c \rightarrow D$  fragmentation) and the solid curve includes fragmentation effects as simulated by coloured string breaking (the Lund model).

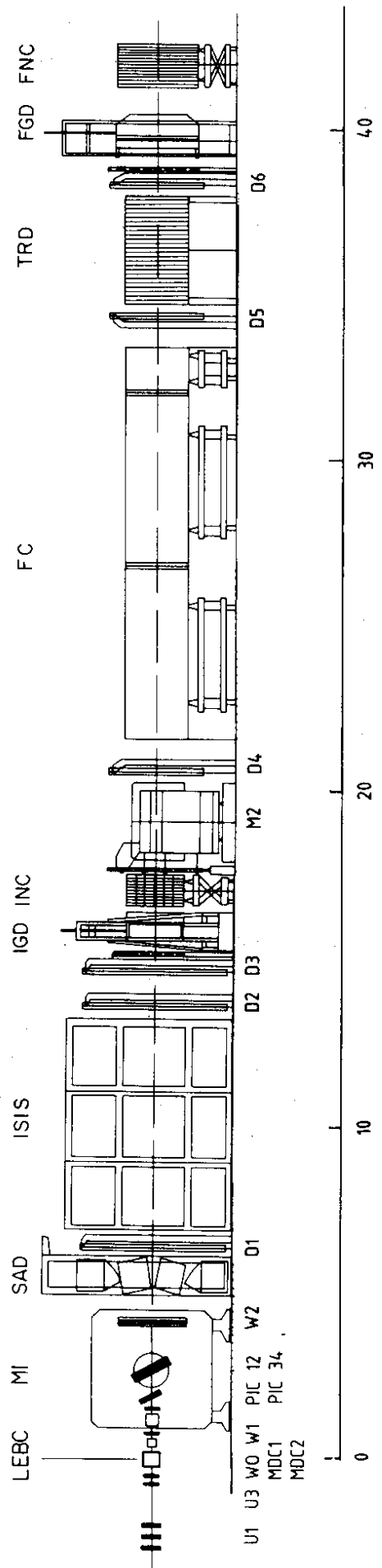


FIG. 1

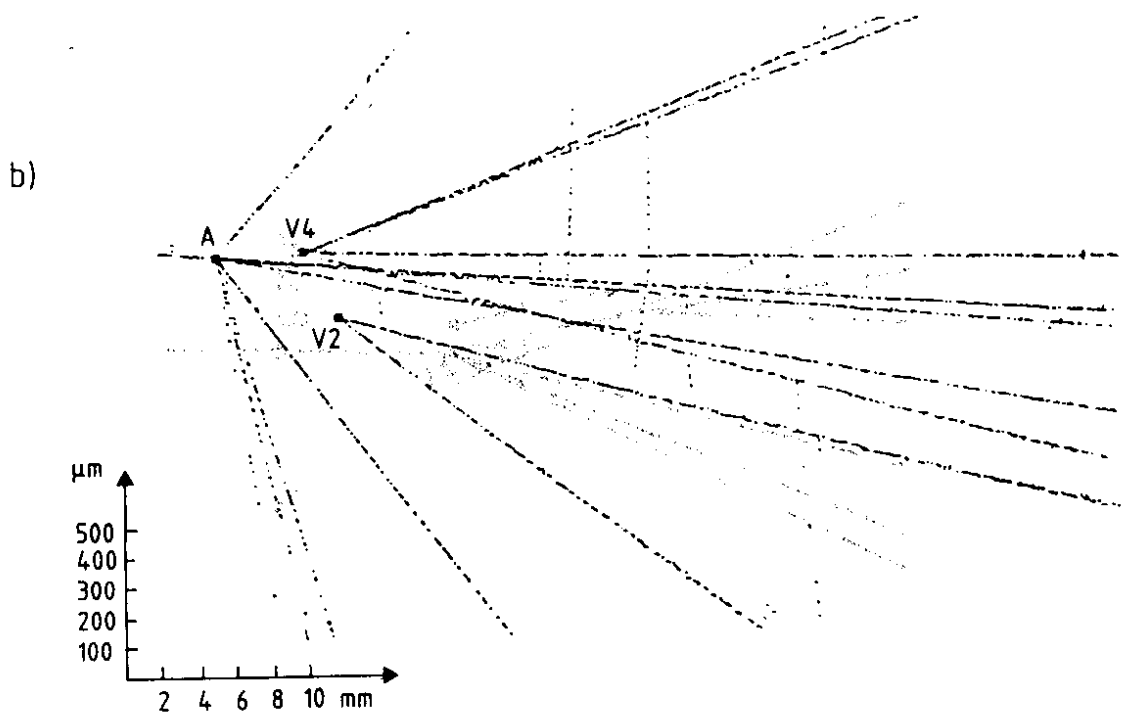
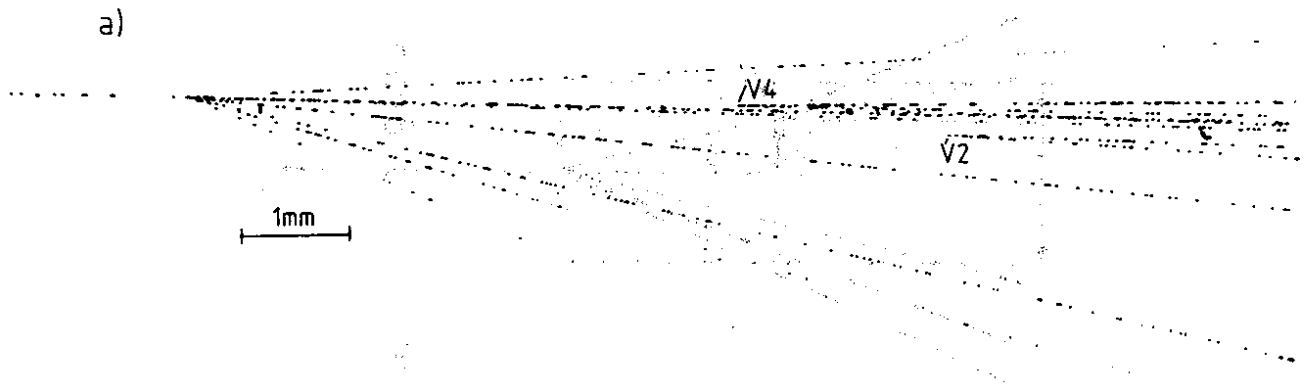
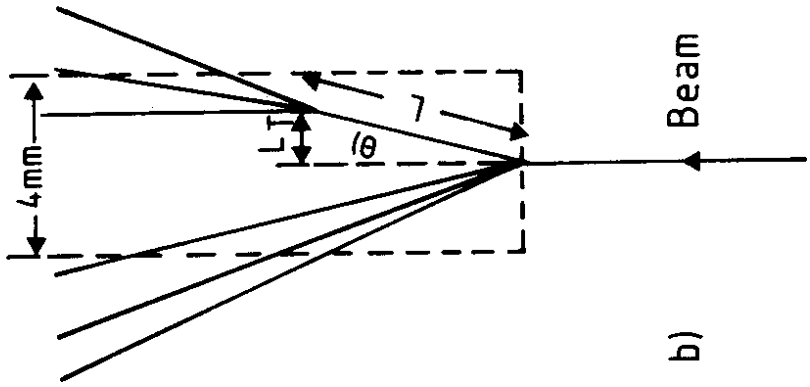
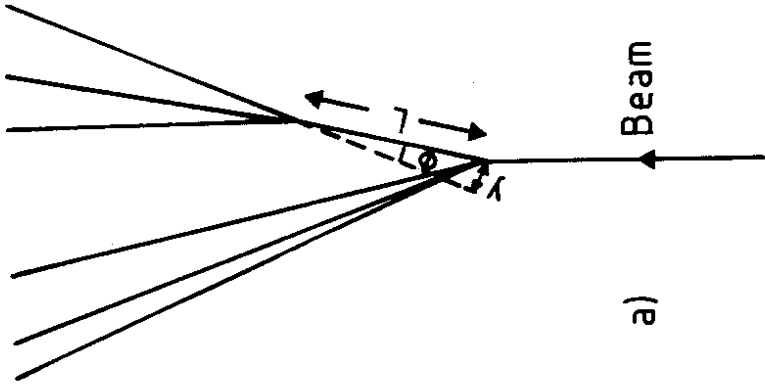


FIG. 2



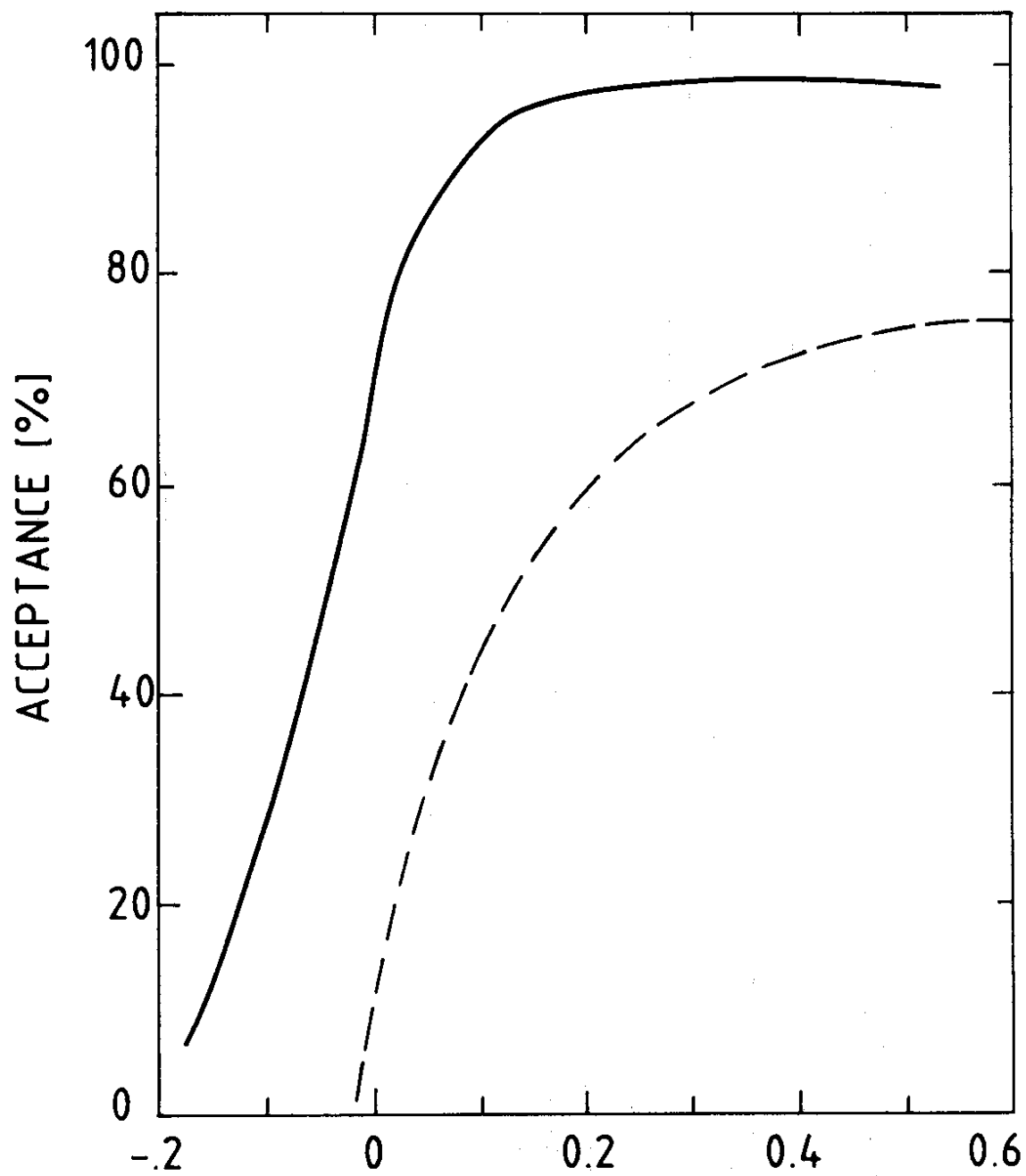
b)



a)

FIG. 3





Feynman - x      FIG. 4

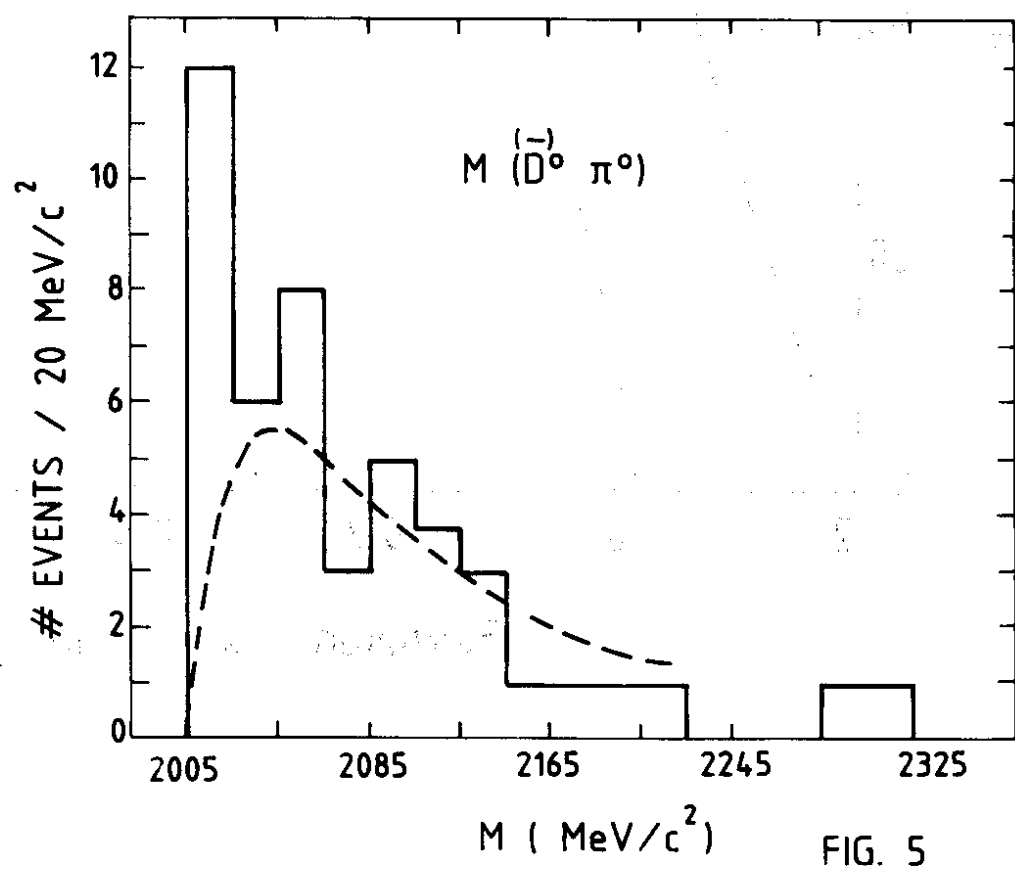
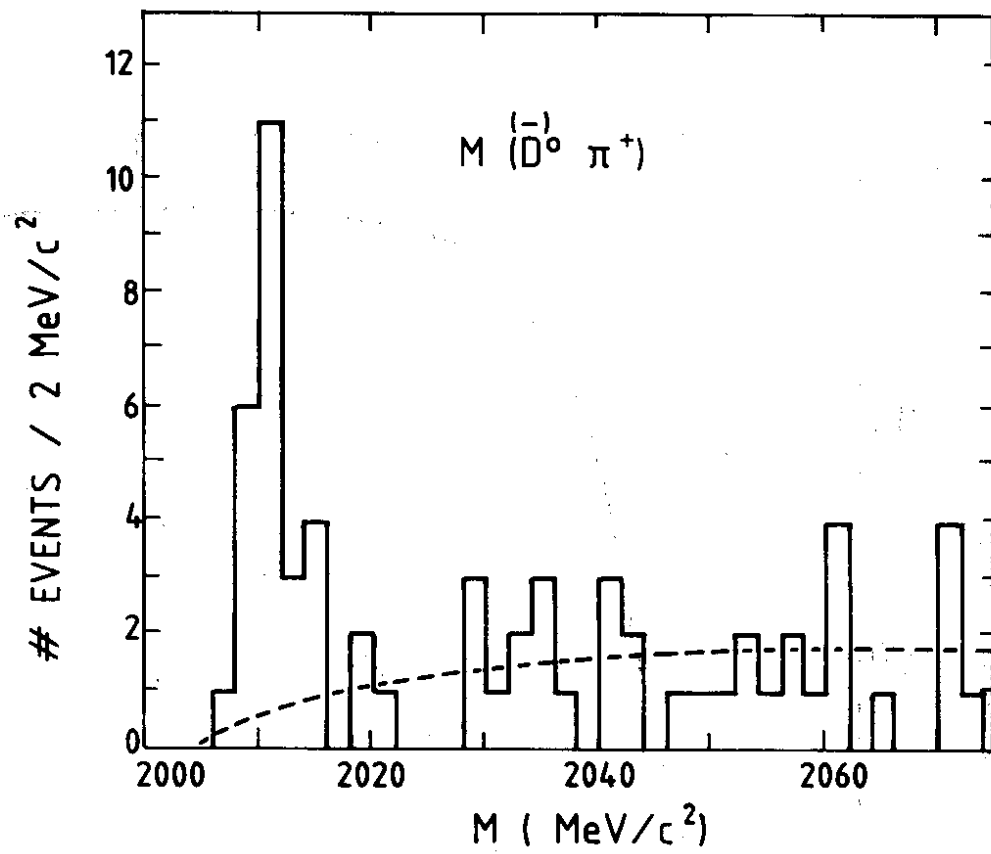


FIG. 5

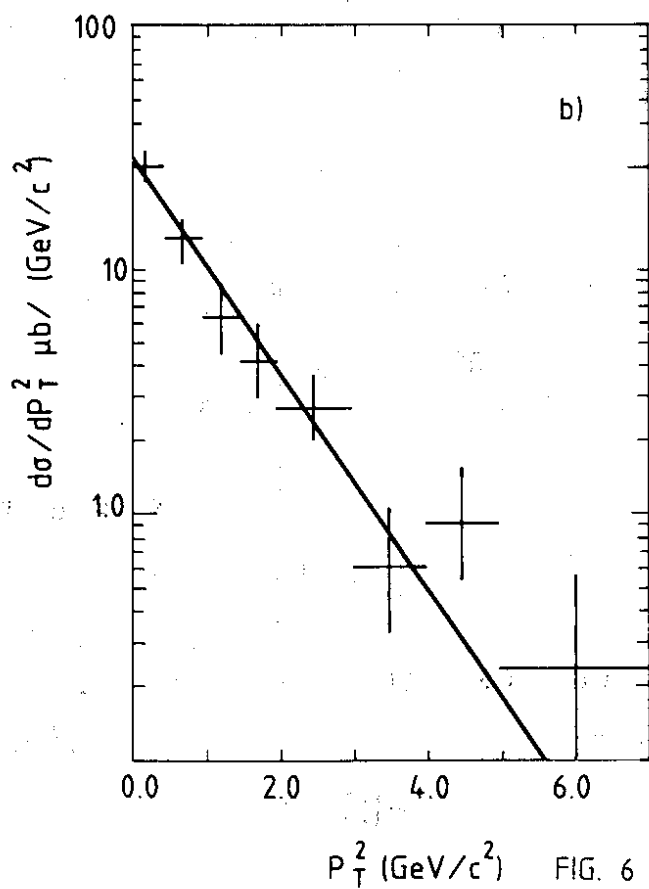
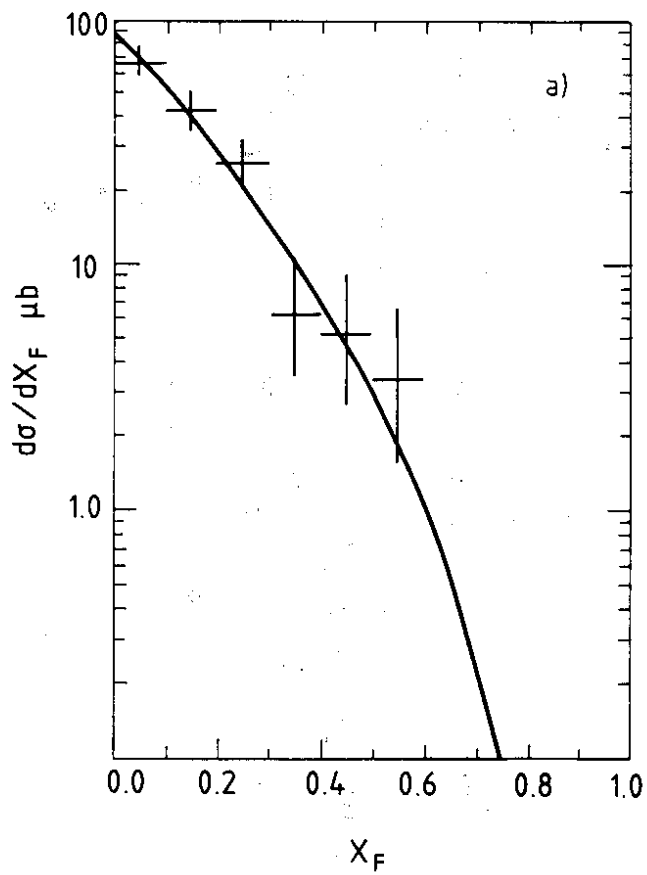


FIG. 6

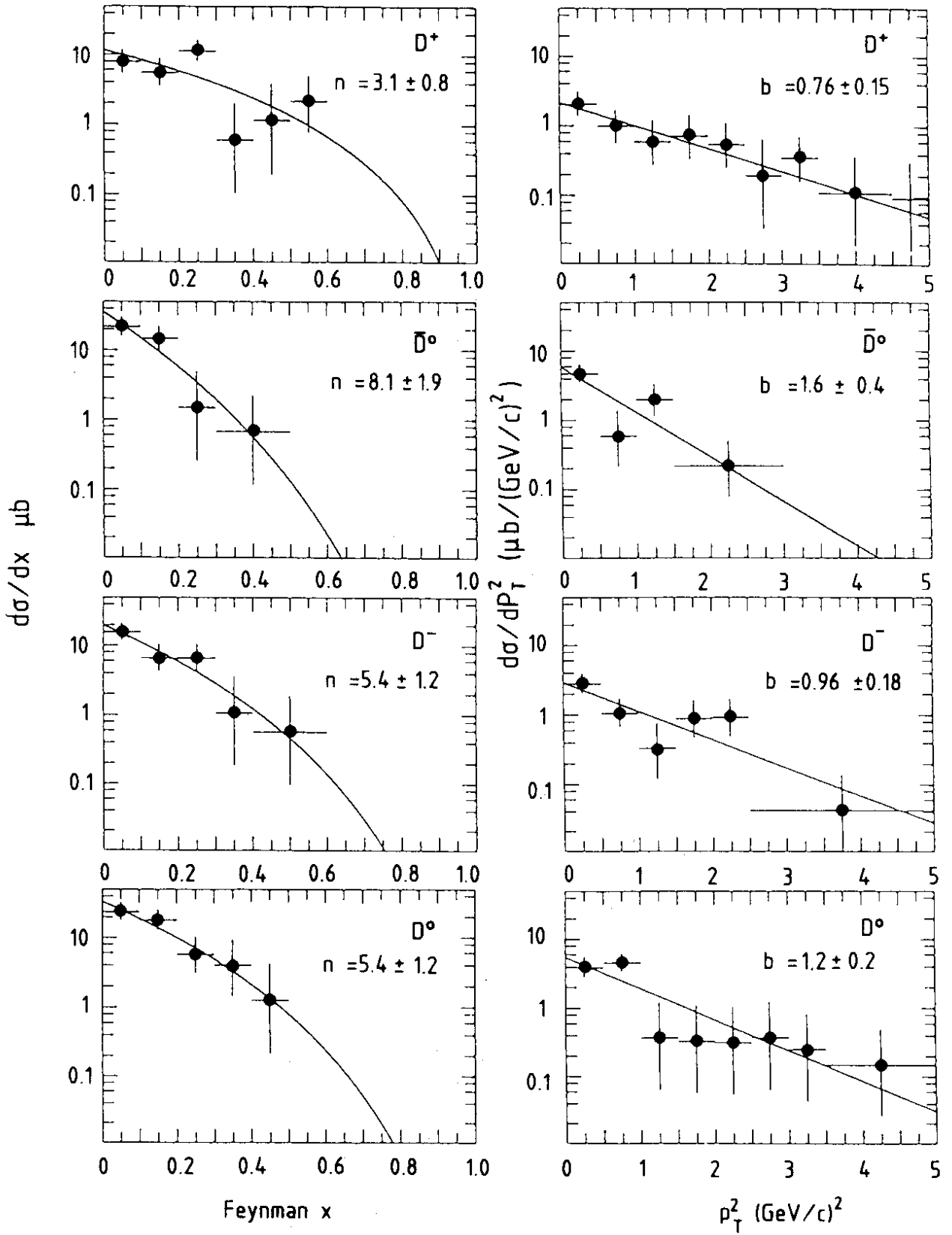


FIG. 7

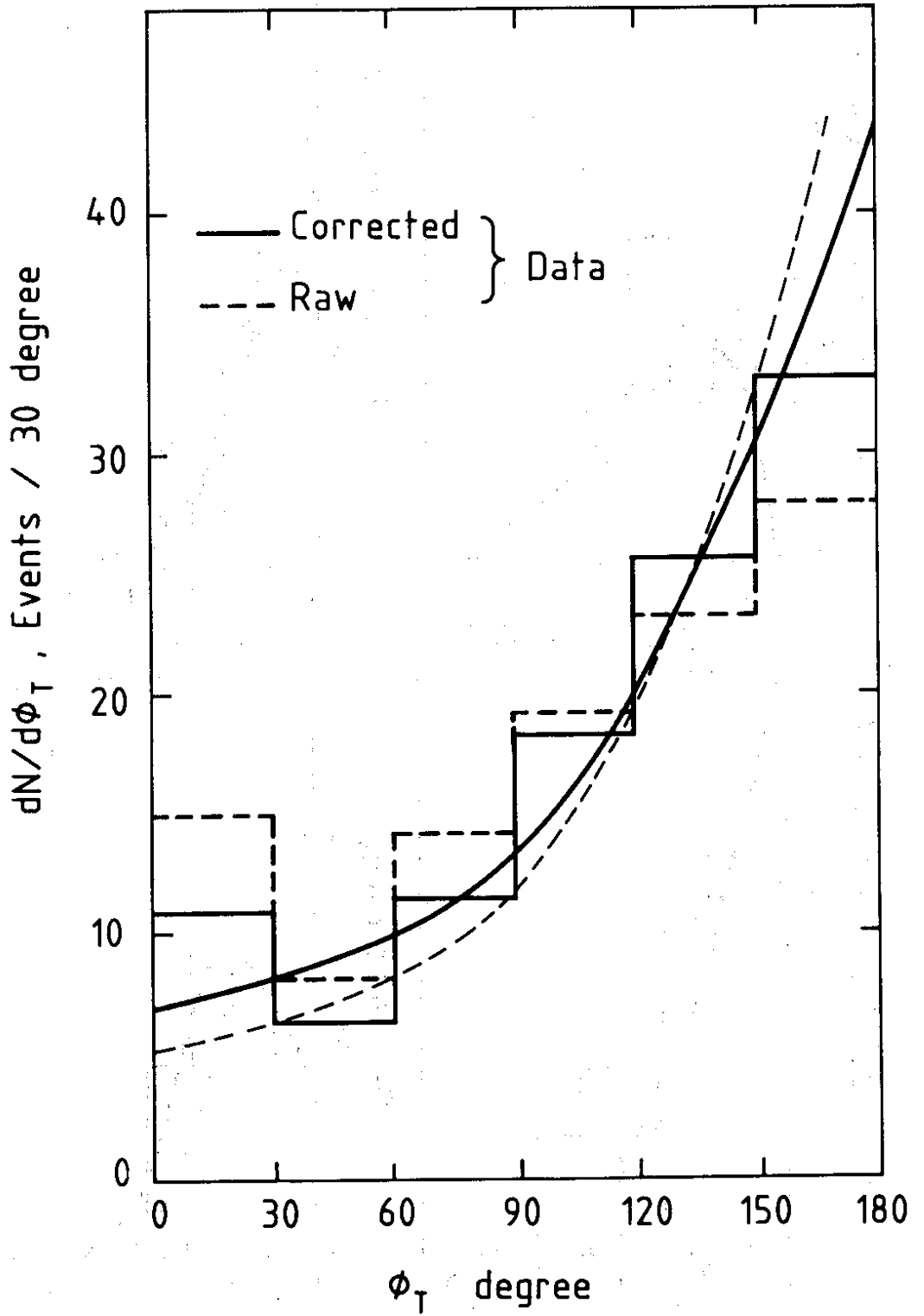


FIG. 8

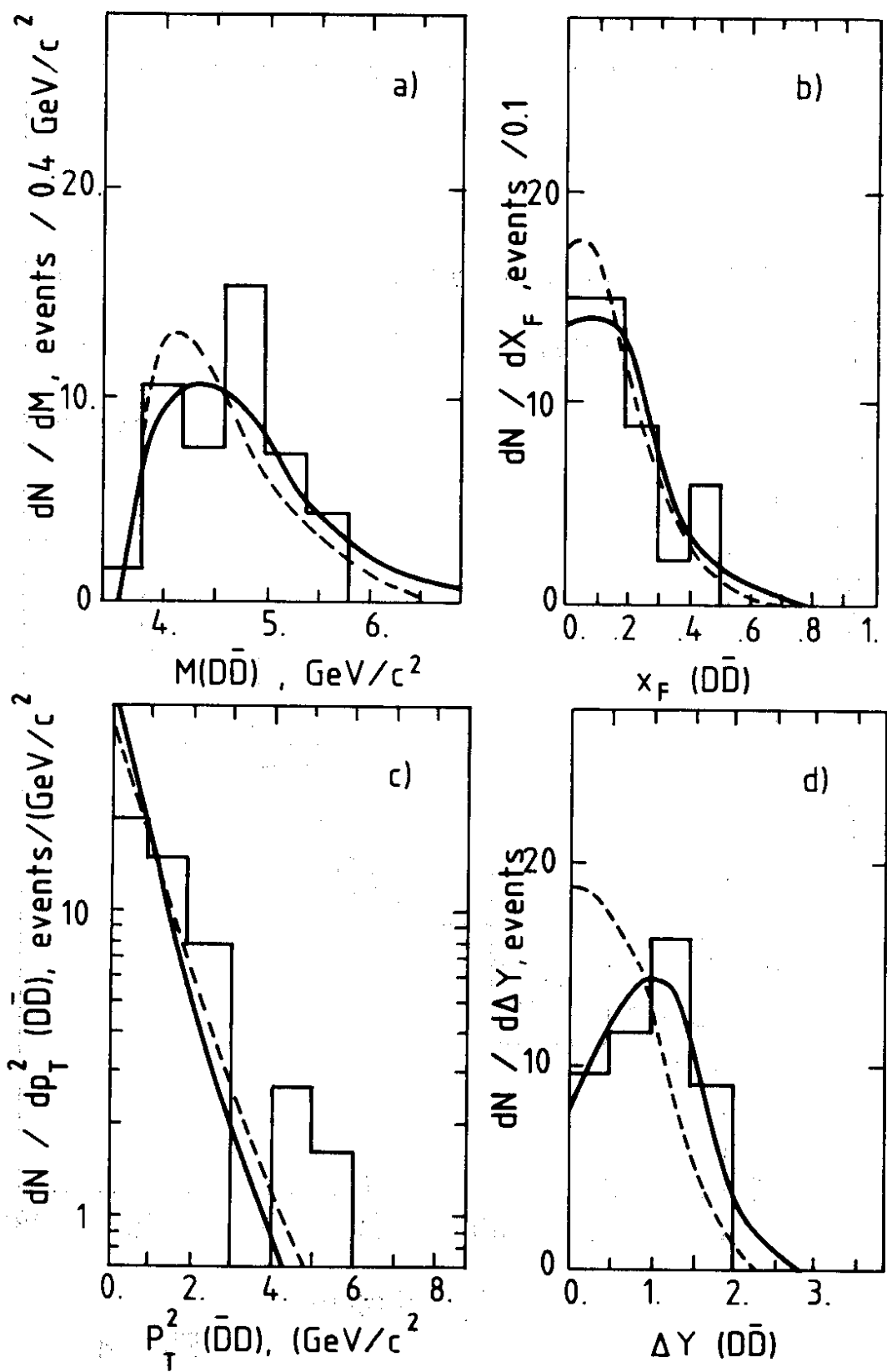


FIG. 9

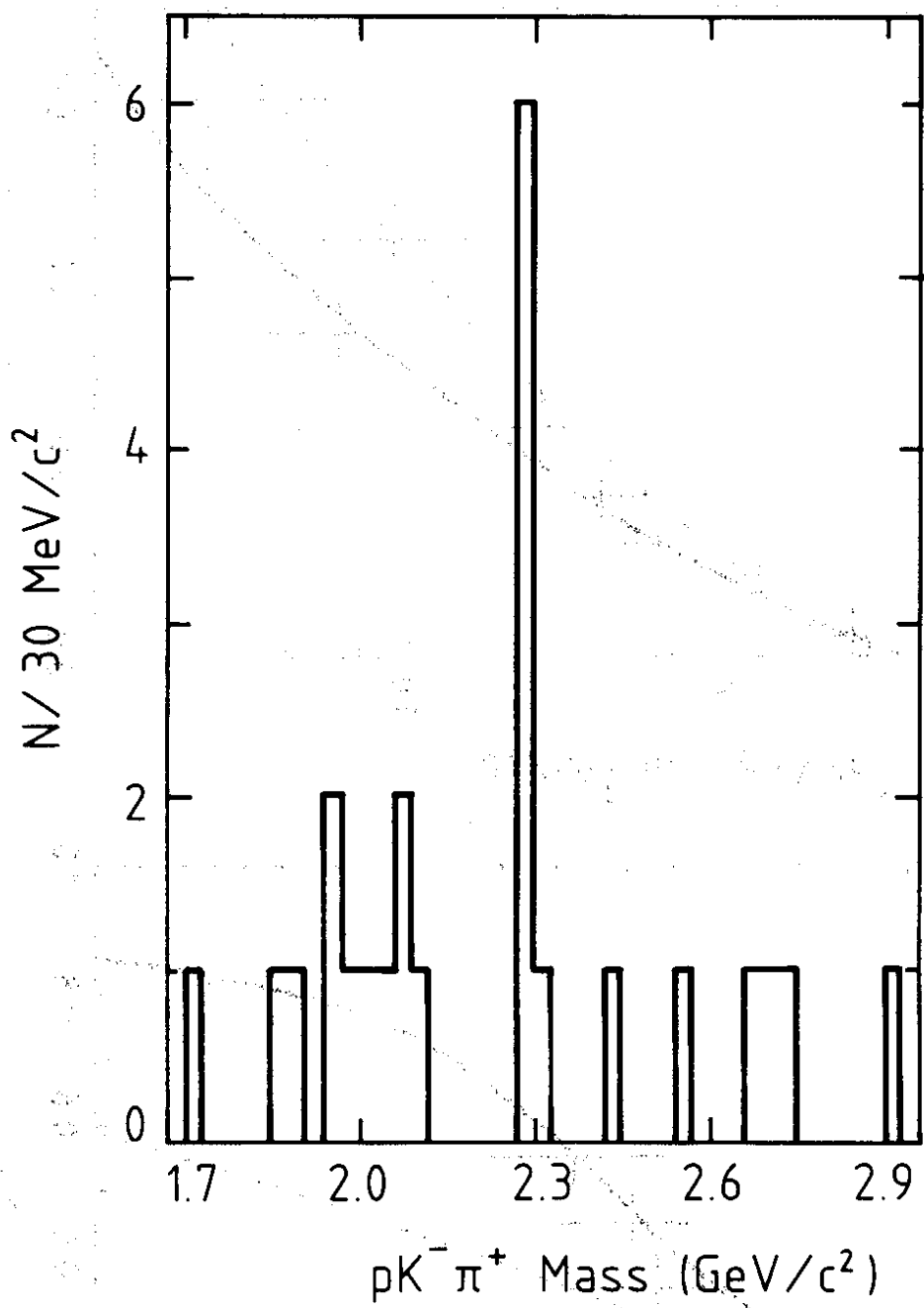


FIG. 10

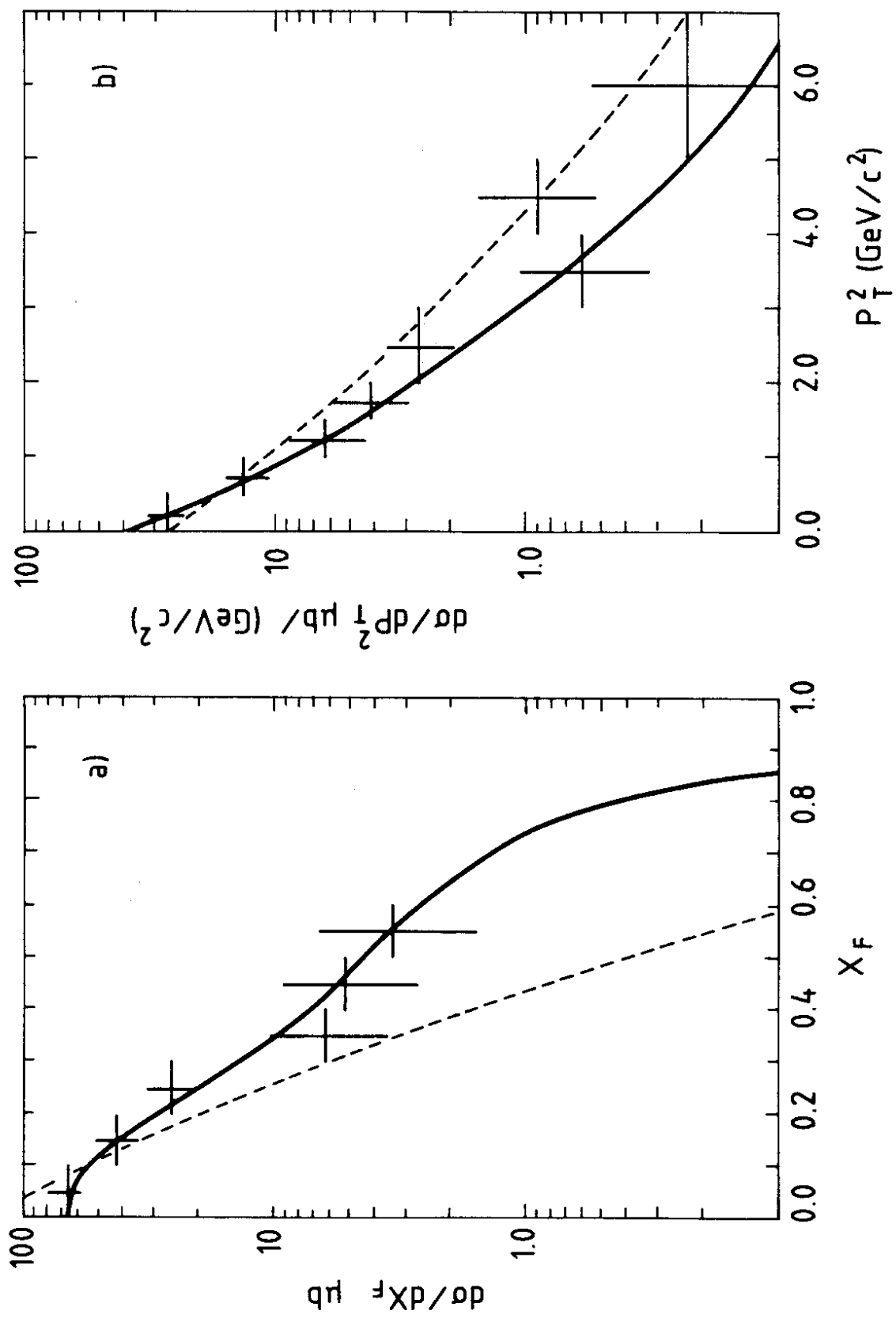


FIG. 11